THESIS

SPATIAL ACCUMULATION PATTERNS OF SNOW WATER EQUIVALENT IN THE SOUTHERN ROCKY MOUNTAINS

Submitted by

Benjamin C. Von Thaden

Department of Ecosystem Science and Sustainability

In partial fulfillment of the requirements

For the Degree of Master of Science

Colorado State University

Fort Collins, Colorado

Spring 2016

Master's Committee:

Advisor: Steven R. Fassnacht

John D. Stednick
Gregory Butters

ABSTRACT

SPATIAL ACCUMULATION PATTERNS OF SNOW WATER EQUIVALENT IN THE SOUTHERN ROCKY MOUNTAINS

Only several point measurements may be taken within a given watershed to estimate snow water equivalent (SWE) due to cost limitations, which necessitates basin-scale estimation of SWE. Modeling often assumes consistency in the spatial distribution of SWE, which may not be correct. Identifying patterns and variability in the spatial distribution of SWE can improve snow hydrology models and result in more accurate modeling. Most previous snow distribution studies focused on small domains, less than 10 km. This study examined SWE distribution at a domain of 757 km.

This study used variogram analysis for SWE data from 90 long-term SNOTEL stations to determine if a physical distance exists at which snow accumulation patterns across the southern Rocky Mountains vary abruptly. The concurrent accumulation period from SNOTEL stations were paired one-by-one until all 90 stations were compared among each other for all years on record. This comparison generated a relative accumulation slope (relative to the accumulation slope of all other 89 SNOTEL stations from the period of record) and along with physical distance between station pairs, variograms were computed using the semi-variance of the relative accumulation slopes. A physical divide (a break in high-elevation terrain) exists in the topography of the study region that runs East-West about the parallel 38°45'N. Two subset variograms were computed, one by dividing station pairs by their location relative the parallel

38°45’N into a north zone and a south zone, and the second by the pair’s land cover type, specifically evergreen, non-evergreen, or mixed.

From the variogram analyses two physical distances were determined (100 and 340 km) at which snow accumulation patterns in the southern Rocky Mountains vary abruptly. There was more variance in snow accumulation south of the 38°45’N parallel, as the zone north of the 38°45’N parallel experiences storm tracks different from the storm tracks that dominate the zone south of this dividing parallel. Land cover was shown to have little effect on snow accumulation patterns. The amount of variability in individual day SWE was found to be correlated to the magnitude of the average SWE among all SNOTEL stations, such that the greater the average SWE, the larger the variability in SWE across the southern Rock Mountains.

ACKNOWLEDGMENTS

First and foremost I would like to thank my advisor Steven Fassnacht for his input and guidance through my undergraduate and master's degree, and in constructing this thesis. I would also like to acknowledge John Stednick for his guidance, Greg Butters for stepping in late as the external member of the committee, and Robin Reich for his input to this thesis. A big thanks goes out to my friends and family who have supported me throughout my education. Partial funding for this research was provided by the Colorado Water Institute (Student Award-2015CO309B), as well as the NASA Terrestrial Hydrology Program (Award NNX11AQ66G, "Improved Characterization of Snow Depth in Complex Terrain Using Satellite Lidar Altimetry," PI Michael F. Jasinski NASA GSFC).

TABLE OF CONTENTS

CHAPTER 1:

Introduction

At the large scale, the mean monthly snow covered area (SCA) across the Northern Hemisphere ranges from 7% to 40% (Hall, 1988). This changes seasonally and from year to year. Data compiled from multiple different sources showed that the March SCA was constant from about 1960 to the early 1980s, then decreased through the 1980s, followed by an increase in the early 1990s and has been stable through 2010 (Brown and Robinson, 2011). However, while the April SCA was similar to March through the early 1990s, it has been decreasing since then (Brown and Robinson, 2011). Such observed shifts in persistent snow patterns could in turn affect water resources.

At the watershed scale, understanding patterns and variability in spatial snow distribution is critical in determining the timing, magnitude and inter-annual consistency of snowmelt runoff (e.g., Molotch, 2009) and when used in concert with such models will ultimately bolster snow distribution model outputs. Typically only several point measurements of snow properties are taken within a given watershed due to cost limitations, yet there is a necessity for basin-scale modeling of snow processes. Such information is crucial for snowmelt hydrology models, including those used for water resource management and forecasting (U.S. Army Corps of Engineers, 1956; Male and Gray, 1981; Martinec and Rango, 1986; WMO, 1986; Kane *et al*., 1991; Sturm and Wagner, 2010).

Patterns are known to exist in inter-annual snow accumulation, as certain locations are known for consistently experiencing lots of snow year in and year out such as Buffalo Pass and Wolf Creek (*Figure 2.1*). The same can be said for locations that consistently experience lower snow accumulation totals. Snow accumulation is also known to be quite variable from year to

year as is evident with the recent lack of snow in California and the Pacific Northwest (Abatzoglou *et al.,* 2014). Fassnacht and Derry (2010) found that in the southern Rocky Mountains a division in climate in terms of snow accumulation exists around the latitude 39 to 40°N in central Colorado. This division is near the boundary of several major watersheds including the Colorado River, the Arkansas River, the Platte River, and the Gunnison River and can be attributed to storm tracks (Changnon *et al*., 1991; Cayan, 1996; Doesken and Judson, 1996; Serreze *et al*., 2001; Bales *et al*., 2006; Deems *et al*., 2006; Fassnacht and Derry, 2010).

Primary factors controlling snow distribution and snowpack properties are precipitation quantities, solar radiation, wind, topography, vegetation, and mass movement by avalanches (Zakrisson, 1981; Elder *et al*., 1991; Trujillo *et al*., 2007; Sexstone and Fassnacht, 2014). Topography only changes over geological time and changes in vegetation are also slow, except for dramatic changes such as forest disturbance. Clearing size, or vegetation density, plays an important role in deposition after redistribution, as well as interception leading to sublimation and melt. The other controlling factors vary intra- and/or inter-annually, but still have some consistency such that strong temporal patterns exist in the distribution of snow (Sturm and Wagner, 2010). Several studies on the topic of snow patterns (König and Sturm*,* 1998; Jansa *et al*., 2002; Anderton *et al*., 2002) observed conditions under which drifting snow and consistent prevailing winds were driving factors of snow distribution. Therefore, the fixed controls of topography and vegetation were a clear source of pattern stability (Sturm and Wagner, 2010). However, determining the inter-annual persistent patterns of the distribution of snowpack properties is difficult as snow cover is the most rapidly varying large-scale surface feature on the Earth (Hall, 1988).

A consistent pattern in a given snow property is a pattern that repeats in relative magnitude in comparison to the same property in the surrounding region inter-annually within a defined scale, and can be physically measured. Molotch and Meromy (2014) used time series SCA data from remotely sensed snow cover data to analyze snow cover persistence (the number of days a given pixel contains snow in a year) in the Sierra Nevada Mountains. From these snow cover persistence maps, the spatiotemporal variability of snow persistence was assessed. They found that while inter-annual patterns occurred in the snow persistence maps, there was also significant inter-annual variability. The authors also looked at seven controlling variables for snow persistence through regression tree modeling and found elevation, precipitation, and temperature to be the most important. Because Molotch and Meromy (2014) evaluated snow persistence in the melt stage, the patterns are several processes removed from patterns that occur in the accumulation stage (the focus of this study).

There is an apparent gap in understanding the level of confidence associated with spatial snow patterns: The small samples of point data relative to the spatial coverage of operational sites and snow courses along with extreme spatial variability in snow properties causes such data to not be representative of the surrounding snow properties and patterns. Winkler and Moore (2006) assessed variability in snow accumulation patterns within forest stands in the interior of British Colombia, Canada. The scale was at the process scale, and the extent of the two study locations was 1 hectare. Three years of snow course data and manual snow water equivalent (SWE) measurements yielded 576 sample points under forest cover and in clearcuts. Year alone was found to account for 33% of the variability in SWE at the study plots, but canopy crown closure explained the largest portion of the variability in April 1st SWE. In all, there have been relatively few quantitative investigations on how closely snow patterns repeat inter-annually, or

how to measure such patterns (Sturm and Wagner, 2010). Thus, this justifies the need to develop methods to quantify repeating patterns in the distribution of snow.

Data used in this study were SWE data collected by the Natural Resources Conservation Service (NRCS) at their operational snow telemetry (SNOTEL) stations. Due to the variable timing of melt at existing SNOTEL stations, as well as between SNOTEL stations, the melt period was disregarded and the period of accumulation is the focus of this study. SWE time series data were used over snow depth because it is the longest daily dataset and because of the practical application for water resources monitoring and modeling. Furthermore, the NRCS SNOTEL network is the most widely available SWE data in the western United States with over 700 operational stations and provides the best spatial coverage of the study region (Sturm *et al.*, 2010).

The hypothesis is that there exists a physical distance between SNOTEL stations at which snow accumulation patterns across the southern Rocky Mountains vary abruptly. The objectives of this study are as follows: (1) to determine the consistency of snowpack accumulation patterns over time for all pairs of SNOTEL stations, (2) if the patterns are consistent, to determine the spatial extent, (3) to define if subsets of stations pairs can better explain spatial accumulation patterns, and (4) to determine how SWE varies for individual dates in the accumulation season. These subsets were based on north-south location and land cover-based characterization. The word “consistent” in the above context is defined as the inter-annual similarity of accumulation patterns between two SNOTEL stations.

CHAPTER 2:

Study Region and Dataset

The study area is the southern Rocky Mountains spanning from southern Wyoming through Colorado to northern New Mexico (*Figure 2.1*). This area is a key region for water supply to millions of people, exhibits persistent snow cover at elevations above 2500 m (Moore *et al.,* 2014), and is the headwater of four major western watersheds, including the Colorado, Platte, Arkansas, and Rio Grande Rivers. This area includes 90 long-term SNOTEL stations operated by the NRCS that collects daily SWE data (*Figure 2.1*). The northern-most SNOTEL is located in the Laramie Range at 42°43'N and the southern-most SNOTEL is in the southern Sangre de Cristo Range at 35° 55'N.

Most of the long-term SNOTEL stations are at elevations that experience persistent snow cover between 2500 m and 3500 m (*Figures 2.1 and 2.2,* and Moore *et al.*, 2014). The highest elevation SNOTEL is Beartown at 3536 m and is located in the San Juan Mountains near Silverton, Colorado. The lowest elevation SNOTEL is Battle Mountain at 2268 m and is located in the Sierra Madre Mountains near Savery, Wyoming. The physical distance between SNOTEL sites ranges from 3 km to 757 km, so the extent of the study domain is 757 km while the support (integration area) of the measurements is 10 m^2 (Blöschl, 1999). The SNOTEL with the largest mean maximum SWE is Tower at 1324 mm and is located on Buffalo Pass near Steamboat Springs, Colorado. The SNOTEL with the smallest mean maximum SWE is Copeland Lake at 144 mm and is located in Rocky Mountain National Park near Allenspark, Colorado. Detailed locations of the SNOTEL stations are not disclosed in this study per request from the NRCS.

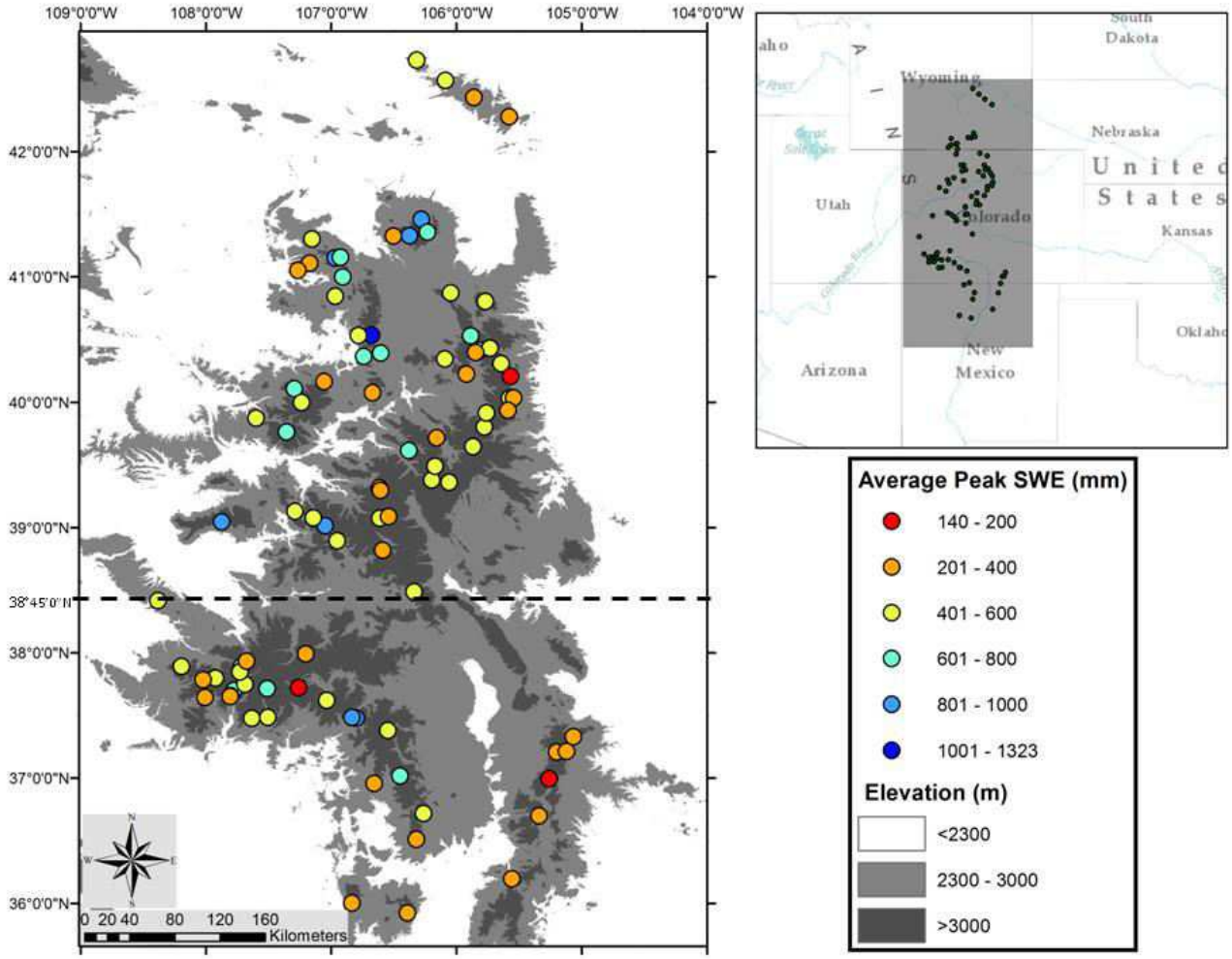

Figure 2.1: Study area of the Southern Rocky Mountains from New Mexico to Wyoming illustrating the 90 long-term snow telemetry (SNOTEL) stations used in the analysis (NRCS).

Precipitation from rain has been known to contribute significantly to annual precipitation totals, such as during the September 2013 floods along the Front Range of Colorado. However, the majority of precipitation in the study region falls as snow with 60 to 75 percent of streamflow resulting from snowmelt in the Rocky Mountains (Doesken and Judson, 1996).

The distribution of SNOTEL elevations of the 90-selected SNOTEL stations in the southern Rocky Mountains poorly represent the actual elevations within the maximum snow-covered extent of the study region (*Figure 2.2* and Fassnacht *et al.*, 2012). For example, there are

no SNOTEL stations located above tree line and so the variability in snow accumulation above tree line is not captured.

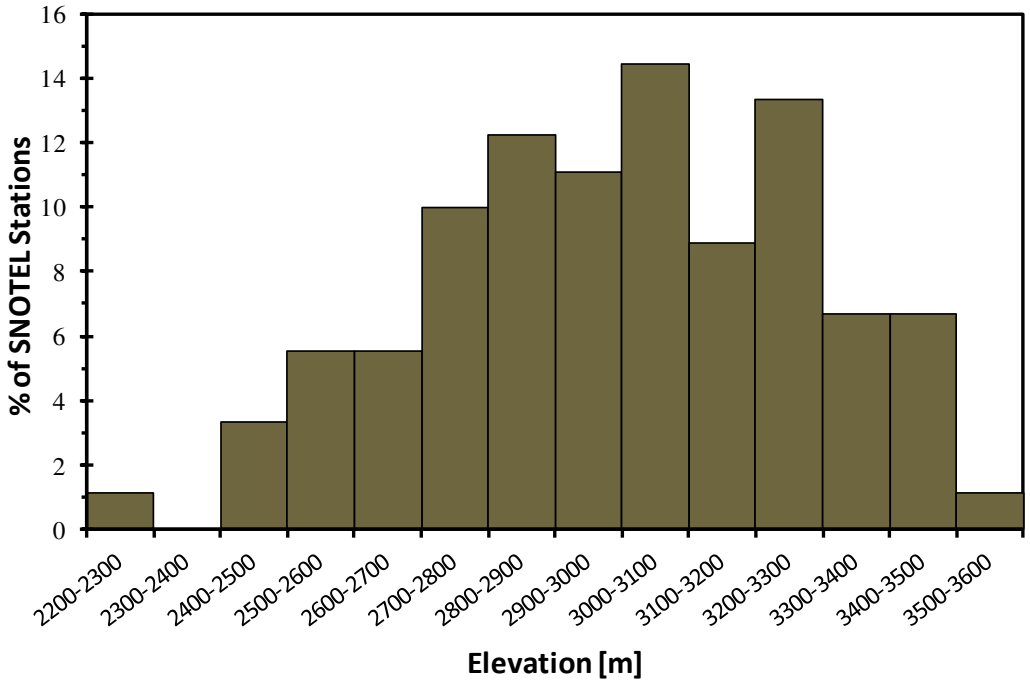

Figure 2.2: Histogram of elevation of the 90 selected SNOTELs in the southern Rocky Mountains.

Elevation has the largest influence on accumulation magnitudes (Fassnacht *et al.,* 2003), but land cover can also have a large effect on both snow accumulation and redistribution. Forest clearings of 1, 2, and 3 H in diameter, where H is the average surrounding tree height, had significantly greater SWE accumulated than other clearing sizes (Golding and Swanson, 1986). Clearing size (open canopy) around SNOTEL stations is not available. However, land cover type around each SNOTEL station is available from the United States Geologic Survey (USGS) National Land Cover Dataset (NLCD) (Homer *et al.,* 2015). The land cover at each SNOTEL fits in one of six categories: developed, deciduous forest, evergreen forest, mixed forest, grassy/herbaceous, or woody wetlands (*Table 2.1)*. For the analysis, each SNOTEL site was

reclassified as either evergreen forest or non-evergreen for all other land cover types, as the remaining land cover types do not have a substantial canopy in the winter.

Table 2.1: Land cover types at each of the 90 SNOTELs used for analysis.

Land Cover Type	% SNOTEL Stations
Evergreen Forest	56%
Grassland/Herbaceous	17%
Deciduous Forest	13%
Mixed Forest	8%
Developed	5%
Woody Wetlands	1%

A subset analysis of this study split the study region in half, due to dominant storm tracks differing for two zones divided by an East-West break in high-elevation terrain (*Figure 1*) at 38°45'N. Several dominant storm tracks take a Pacific frontal track that moves into the study region from the west, northwest, or southwest. Upslope events also contribute to annual snowfall totals along the Colorado Front Range in which the storm track moves north from the Gulf of Mexico (Barry, 2008). This analysis was based on results from Fassnacht and Derry (2010) who found differing climatic sub-regions analogous those in *Figure 2.1*. Such differences were attributed to storm tracks which originate in the Pacific Southwest versus those that originate in the Pacific Northwest and how these different storm tracks tend to see snow accumulate at differing magnitudes about this 38°45'N parallel (Fassnacht and Derry, 2010). The more easterly mountain locations in Colorado also experience snow accumulation from upslope storms (Fassnacht and Derry, 2010).

In pairing SNOTEL stations the distance between station pairs is considered: *Figure 2.3* shows that the distribution in distance among station pairs is slightly right-tailed, with the most station pairs falling within 20 to 400 km distance with many between 80 and 180 km. This right-

tailed distribution was considered, but had little influence on the bin widths of variograms constructed in the results. Due to the maximum spacing between SNOTEL stations (757 km), and the distribution of distances between all station pairs (*Figure 2.3*) the appropriate bin width was set at 20 km.

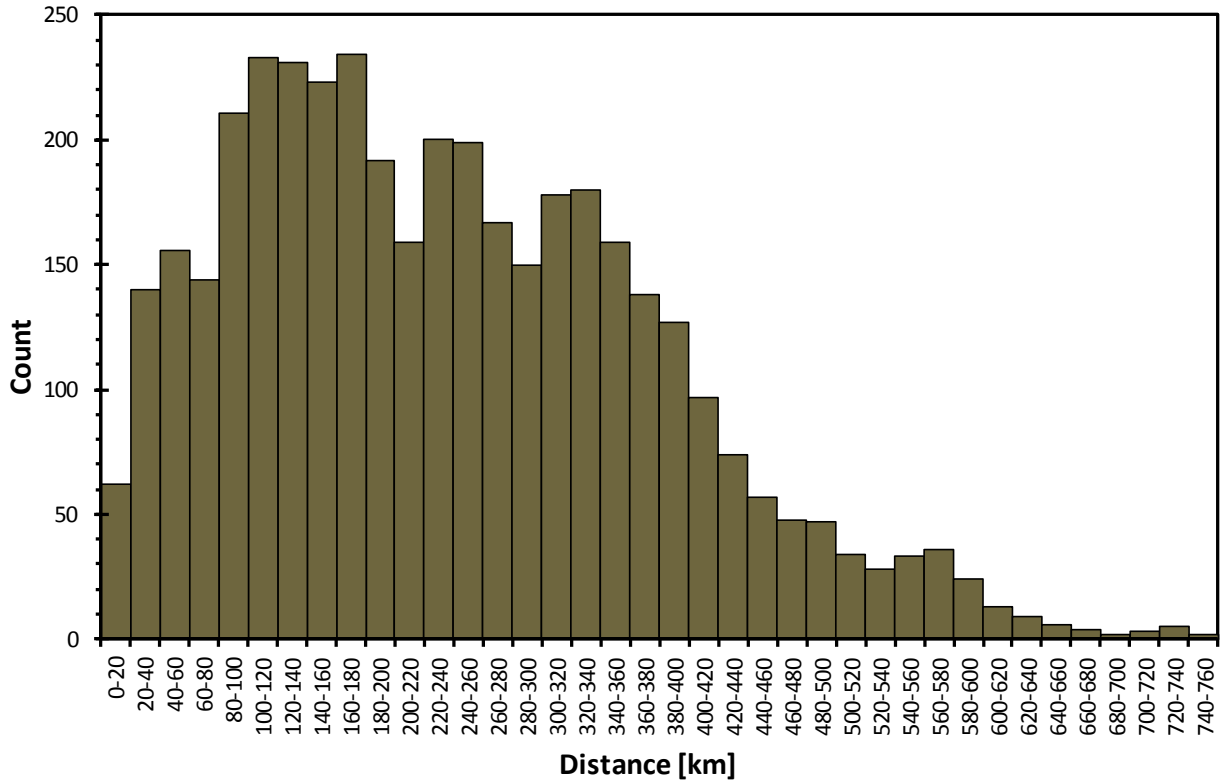

Figure 2.3: Histogram of distance between all SNOTEL pair combinations in the southern Rocky Mountains.

The SNOTEL dataset were used to analyze the comparable snow accumulation rates throughout the contiguous southern Rocky Mountains. From the total 145 SNOTEL stations located in the study area, 90 have a period of record of at least 26 years of daily SWE measurements. Some SNOTEL stations started operating in the late 1970s with the earliest data used in this study being 1982, yielding 32 years of record. The data were obtained from

Fassnacht and Records (2015), and have been quality controlled as per the criteria for SNOTEL data outlined by Serreze *et al*., (1999).

CHAPTER 3:

Methods

Variograms were constructed from relative accumulation slopes between SNOTEL station pairs and inform of the scale of spatial variability in accumulation. Specifically, each SNOTEL SWE time series was compared to all of the other 89 station's SWE time series for each snow year during concurrent accumulation (*Figure 3.1 step 1*). The comparable period of accumulation begins when both station pairs are accumulating, i.e., SWE is increasing (*Figure 3.1 step 2)*, and ends when one of the stations has reached its maximum annual SWE, after which melt begins (*Figure 3.1 step 3).*

To standardize the comparison of each SNOTEL station pair, the station with the larger mean maximum SWE was set as the independent variable for the computation of relative accumulation slopes (*Figure 3.1 step 4*). The accumulation slopes are considered relative because it is derived from a given SNOTEL relative to another SNOTEL comparison. Conceptually, the relative accumulation slope is computed by setting one station as the independent variable, the other as the dependent variable, and plotting SWE values measured on the same day for a given accumulation period (*Figure 3.2 a*). Next, a linear regression using ordinary least squares is applied to the data and the associated slope is computed for each year of snow accumulation (*Figure 3.1 step 5*). For example, the relative accumulation rate between the Niwot and University Camp SNOTEL stations for 1982 is 0.84 (*Figure 3.2 a*). After a relative accumulation slope is computed for each year on record, the semi-variance of these relative accumulation slopes is computed and referred to as slope semi-variance (*Figure 3.1 step 6*). Finally, after all 4005 slope semi-variance values were calculated, they were plotted versus

distance and averaged per 20-km bin (*Figure 3.1 step 7*). Variograms utilize lag distances in which semi-variance data is averaged into bins (Isaaks and Srivastava, 1989).

Deems *et al.* (2006) examined scale breaks in snow depth data at the process scale using variograms. Similar to previous studies (e.g., Shook and Gray, 1995; Deems *et al.,* 2006) the lag distance at which a scale break occurs is determined through identifying abrupt changes in the rate of variance increase on a variogram. This same method was used to identify scale breaks in this study. Lag sections are composed of binned data points that are consecutive up until a scale break. For example, the variogram in *Figure 3.1 step 7* has three lag sections (green, blue, and purple).

In this study, some station pairs exhibit small variance in relative accumulation slopes (*Figure 3.2 a and b*), and others exhibit larger variance in relative accumulation slopes (*Figure 3.2 c and d*). As is such, variograms in log-log space help display all of the data on one plot as well as allow the fitted power functions to appear linear and aid in identifying scale breaks (*Figure 3.1 step 7*). In other words, the variograms are displayed in log-log space because the semi-variance in accumulation slopes increases very quickly at certain lag distances, sometimes by an order of magnitude. This is consistent with the methods used by Deems *et al.* (2006).

As a rule of thumb, any bin with fewer than 20 station pairs was omitted when fitting functions in the variogram plots, although these points still appear on the variogram plots (small sized points). Deems *et al.* (2006) used a similar technique in not including bins at the shortest and longest lag distances as they were considered outliers and were not included when fitting functions to the data.

Subsequent variogram analysis subdivided station pairs that were considered more similar in terms of location and land cover type in order to identify driving processes that

influence scale breaks. The first subdivision split station pairs into north and south zones at the 38°45'N parallel. This divide was chosen due to different SNOTEL-based snow climatologies on either side of this parallel, as well as a natural topographic divide about this parallel for which there is very little land above 3000 m (Fassnacht and Derry, 2010; and *Figure 2.1*). For this first subdivision a location-based variogram was constructed using station pairs in the same zone. Specifically, the north zone was all station pairs north of the 38°45'N parallel, and the south zone was all station pairs south of this parallel. All station pairs on opposite sides of the dividing parallel were labeled "mixed" zone pairs and their data also appear on the location-based variogram (*Figure 4.3*).

The second subdivision was based on land cover, as it influences the distribution of snow (Zakrisson, 1981; Elder *et al.*, 1991; Trujillo *et al.,* 2007; Sexstone and Fassnacht, 2014). All SNOTEL stations have an associated land cover: evergreen forest, deciduous forest, mixed forest, developed, grassland/herbaceous, and woody wetlands (Homer *et al.,* 2015). Station pairings were made based on the evergreen forest land cover type: Each station pair was marked as an evergreen pair if both stations were evergreen forest, a non-evergreen pair if neither station was in evergreen, or a mixed pair if one of the two stations was evergreen. The evergreen land cover type was used to distinguish station pairings because of the interception potential compared to the other land cover and vegetation types. Separate data series were plotted on the land cover variogram for each of the three land cover types (*Figure 4.5*).

Two additional SWE-variograms were constructed based on daily SWE values using the same method as Deems *et al.,* (2006). These variograms did not incorporate accumulation rates but were constructed to examine how SWE varies for specific dates in the accumulation season. The first variogram used SWE data from four dates (3/1/1997, 2/14/2002, 2/9/2011, and

12/22/2012) based on the last day all 90 stations were in accumulation for the winters 1997, 2002, 2011, and 2013. 1997 was the highest accumulation year on record, followed by an average year in 2011, a relatively low accumulation year in 2002, and the lowest accumulation year in 2013. This variogram was constructed by comparing daily SWE values at all 90 station pairs and calculating the semi-variance between each station pair. The semi-variance data were then averaged per log-width bin to yield the variogram plot (*Figure 4.6*). The second variogram examined the 1996-1997 accumulation season daily SWE data from four dates: 11/30/1996, 12/25/1996, 1/16/1997, and 3/1/1997. The binned SWE semi-variance was divided by the square of the average SWE of the given date in order to standardize the relative magnitude of the SWE semi-variance data (*Figure 4.2*). This shows patterns in the SWE semi-variance data that are very similar throughout the extent on all four dates. Lastly, these two variograms were examined for scale breaks and general patterns.

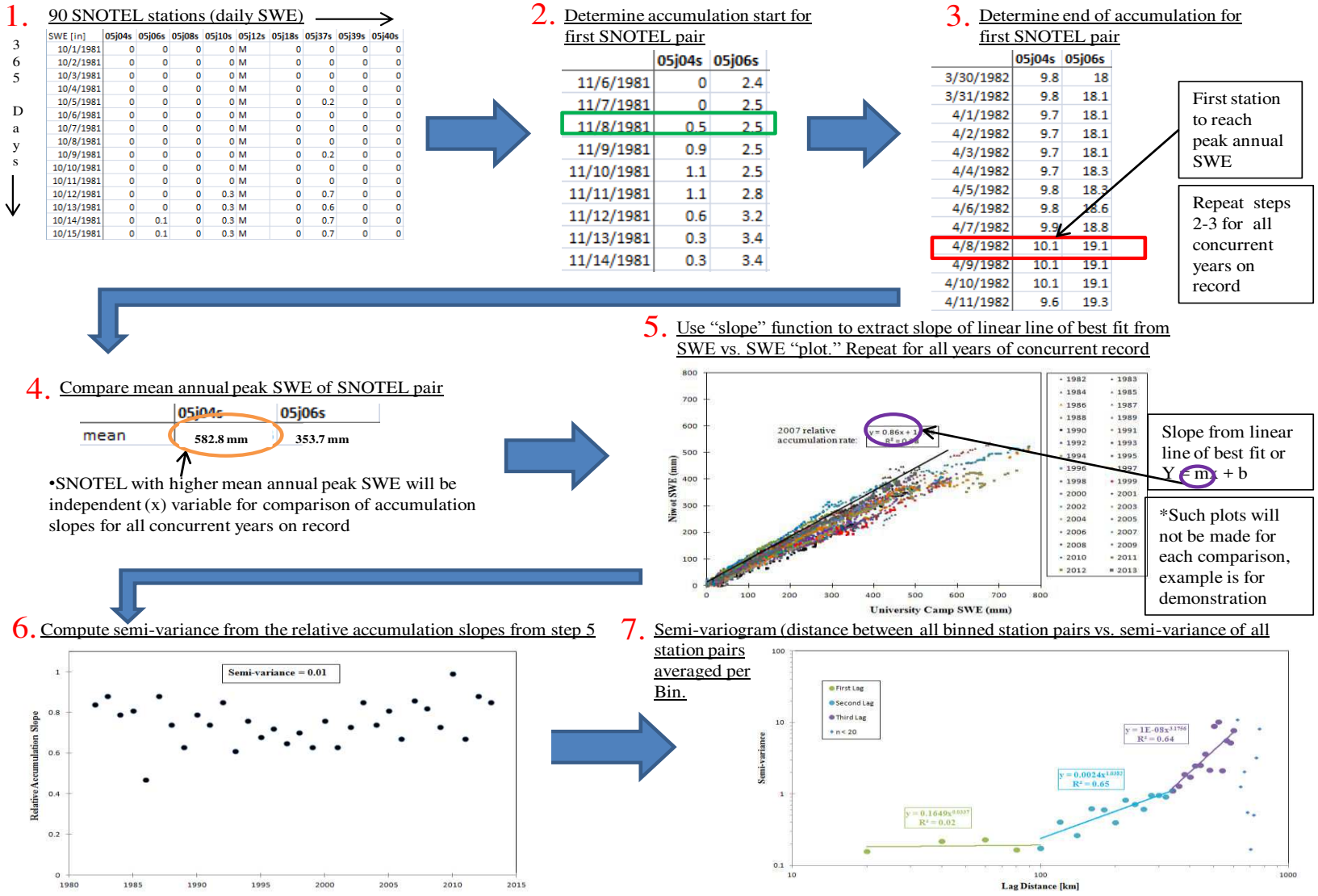

Figure 3.1: Analysis flow of the methodology producing the slope-based variograms. Steps 1through 5 show the example SNOTEL station pair of Niwot and University Camp, further illustrat4ed in Figure 3.2.

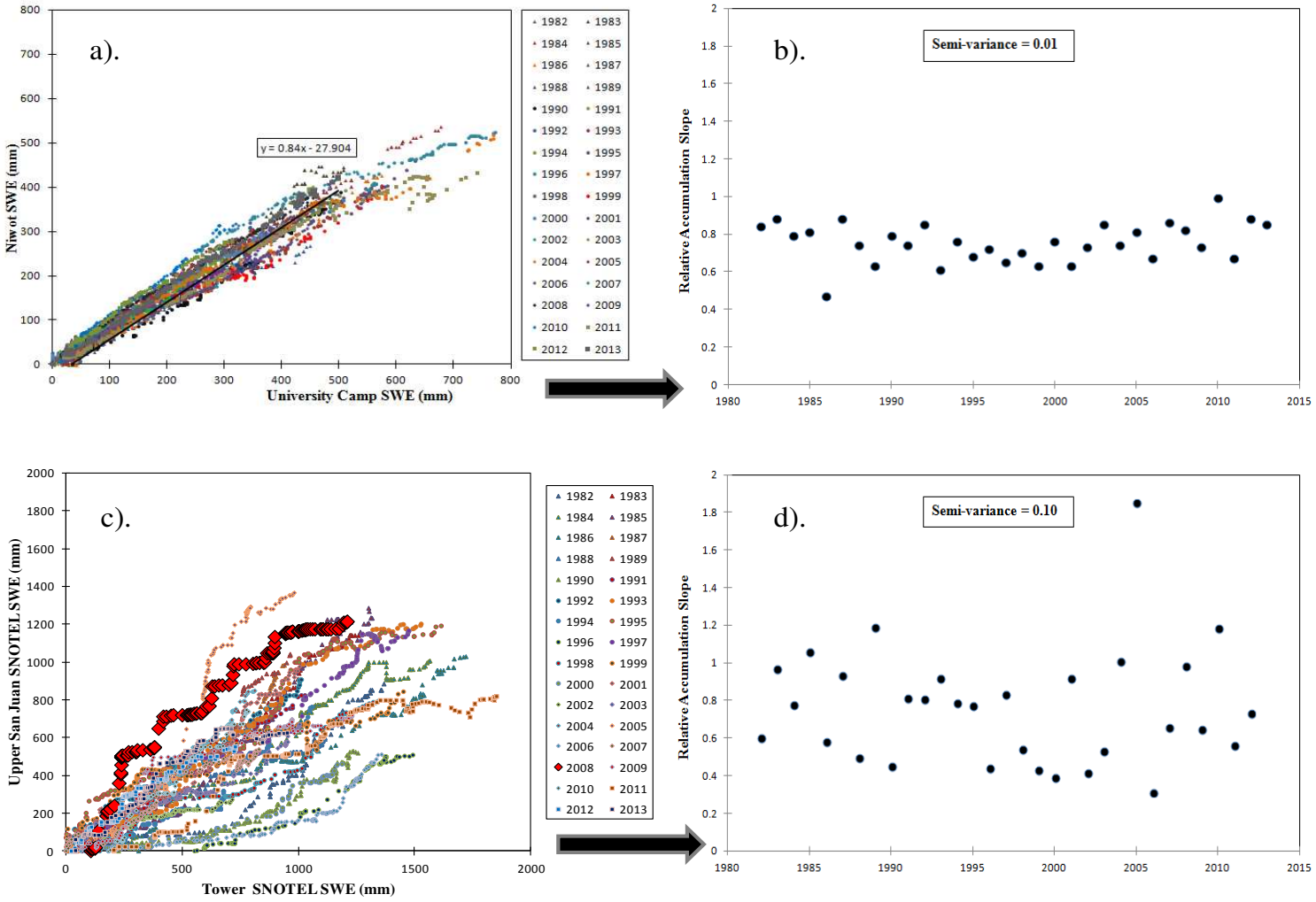

Figure 3.2: Data for relative accumulation slopes for the period of record between a) Niwot and University Camp, and c) Upper San Juan and Tower SNOTEL pairs, as well as plots of semi-variance of these two station pairs, b), and d), respectively. Sub-plots a) and b) show a station pair with low semi-variance and sub-plots show a station pair with higher semi-variance.

CHAPTER 4:

Results

Using all 4005 slope variance values there is much spread in the slope semi-variance data as seen by the high variability in the best-fit curve with an R^2 value of 0.25 (*Figure 4.1*). While variance does increase, there is no obvious scale break illustrated by an abrupt change in the slope semi-variance values. The fitted power function shows a less than linear increase with an exponent of 0.87.

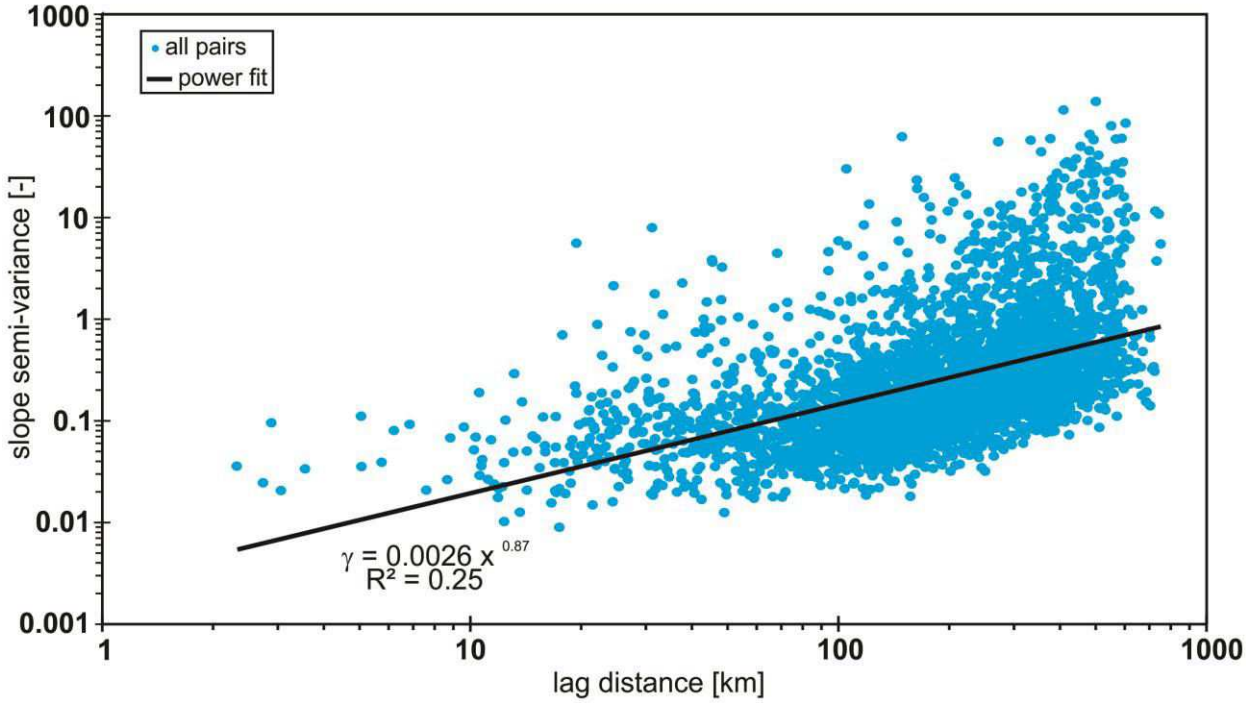

Figure 4.1: Plot of slope variance of accumulation slopes between all station pairs versus lag distance plotted on log-log axes, with a power function fit to the data.

A variogram is usually generated from grouping all station pairs within a specific distance range and averaging the semi-variance per bin; (*Figure 4.2)*. The same general pattern is seen, a pattern of increase with lag distance (*Figure 4.2*). The variance increases more quickly for the binned data (*Figure 4.2*) than the un-binned (*Figure 4.1*) as illustrated by the exponent

(slope in log-log space) of the fitted power function of 1.27 (binned in *Figure 4.2*) versus 0.87 (un-binned in *Figure 4.1*).

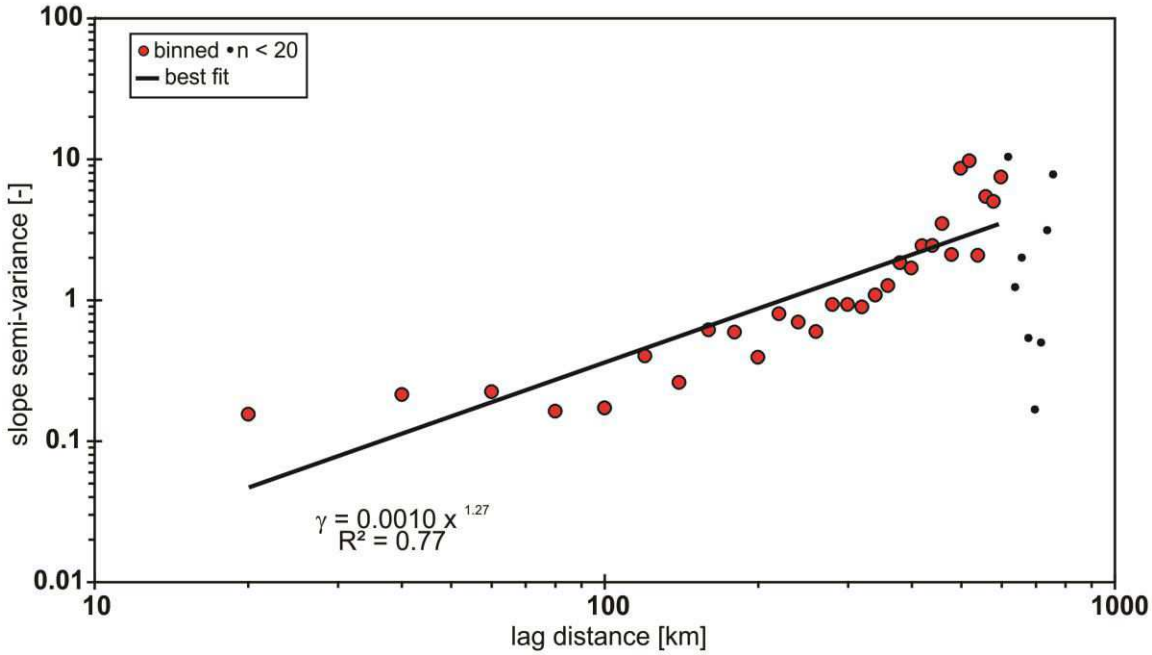

Figure 4.2: Variogram plot of all station pairs on log-log axes with a power function fit. Black points are bins containing less than 20 station pairs and were excluded from the fitted power function calculation.

While a single power function fits the slope semi-variance data relatively well, it underestimates at low and high lag distances and overestimates in the middle (*Figure 4.2*). Three separate fitted power functions, or lag sections, that are divided by two scale breaks, fit the data better (*Figure 4.3*). These scale breaks occur at approximately 100 and 340 km (*Figure 4.3*).

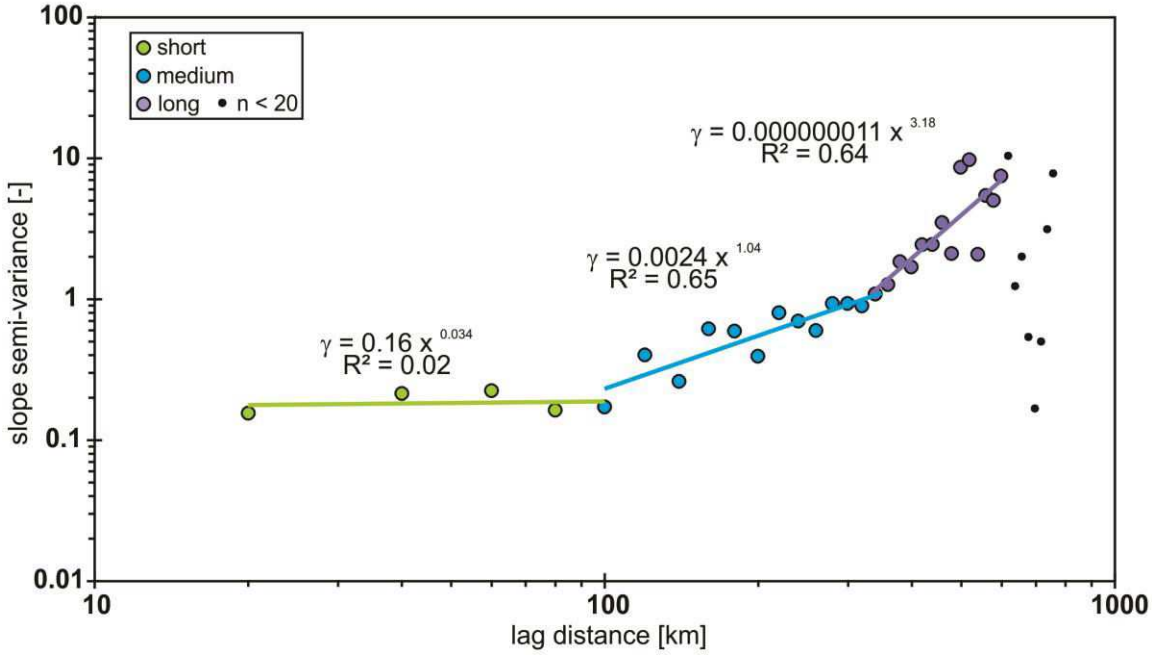

Figure 4.3: Variogram plot of all station pairs on log-log axes with the power functions fitted to data bins containing greater than or equal to 20 station pairs and with three lag sections divided at scale breaks. The remaining black data points beyond 630 km contain less than 20 station pairs per bin.

The subset variograms exhibit spatial accumulation patterns similar to the patterns in the all pairings variogram (*Figure 4.3* versus *Figure 4.4* or *4.5*). Separating the SNOTEL pairs by location, scale breaks were found at 100 km in the north zone and south zone stations (*Figure 4.4*). All three pairings (north, south, and crossed) have different slopes (*Table 4.1).* Creating subset SNOTEL pairings by land cover type exhibits scale breaks in all three land cover types at 100 km lag distance (*Figure 4.5* and *Table 4.1*).

Table 4.1 summarizes the lag distance at which scale breaks were found, as well as the exponents of the power functions fitted to individual lag sections. The exponent of the power functions of the semi-variance is different for the north, south, and crossed zone stations, as separated by the 38°45'N parallel. A scale break may exist in the north zone at 280 km (*Figure 4.4*). This possible scale break is less certain than the scale breaks in *Figure 4.3* because the furthest binned lag distance is 320 km and there are not enough bins beyond 280 km to confirm

an abrupt increase in variance. The difference in semi-variance between the north zone and south zone illustrate the differing climatology about the 38°45'N parallel: If these two zones experienced the same climatology they would have the same magnitude of semi-variance across all lag distances during accumulation.

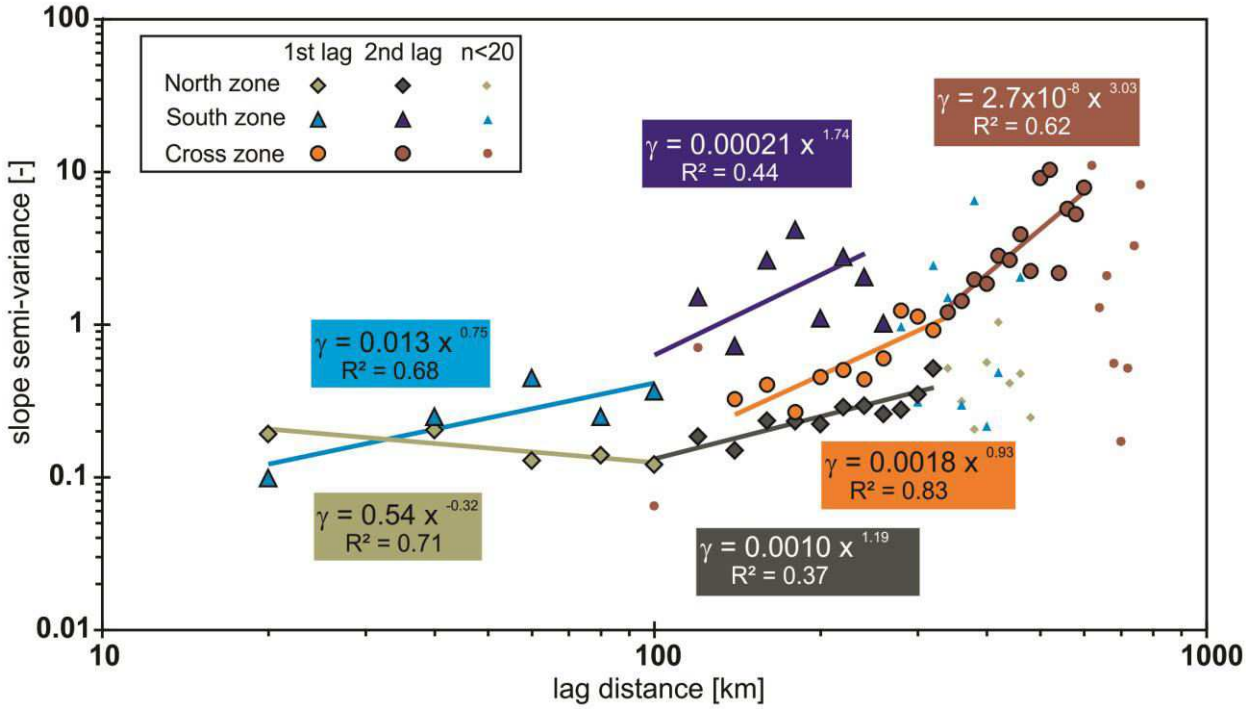

Figure 4.4: Variogram split up by north zone station pairs (tan diamonds), south zone station pairs (blue triangles), and cross north-south station pairs (red circles) with the power curves fitted to data bins containing greater than or equal to 20 station pairs.

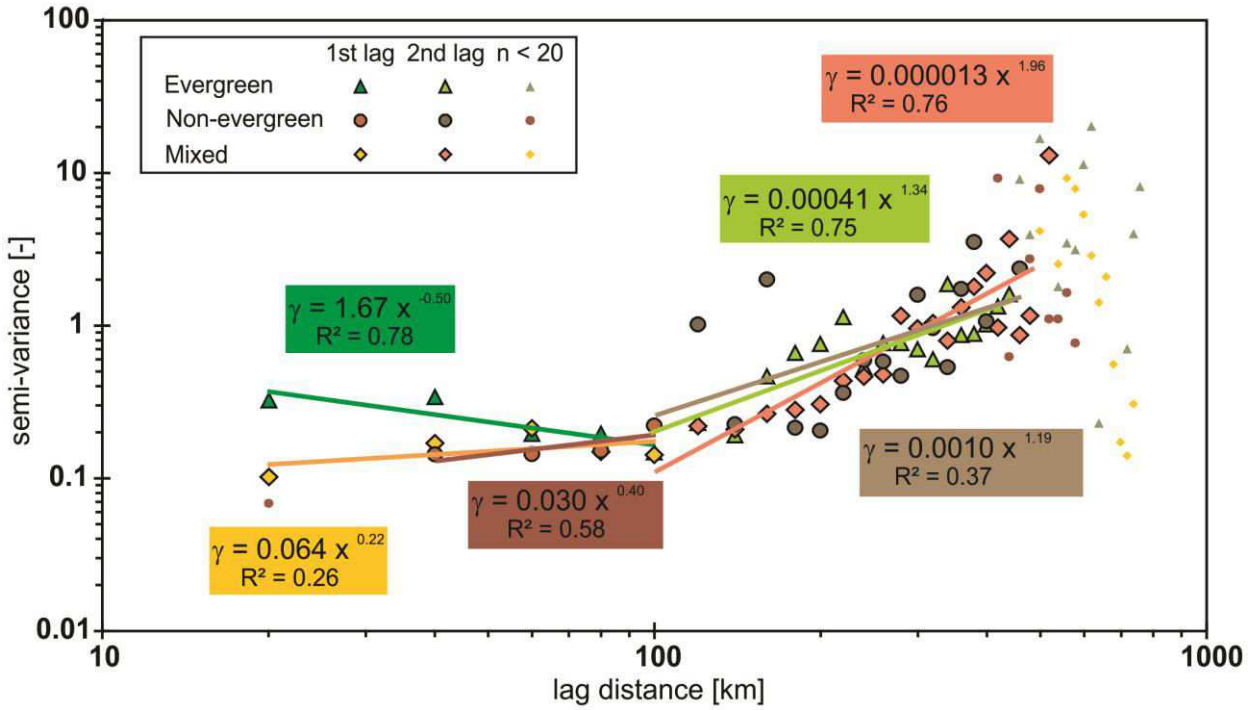

Figure 4.5: Variogram plot of station pairs divided by land cover class (evergreen, mixed, and non-evergreen) on log-log axes with the power functions fitted to data bins containing greater than or equal to 20 station pairs.

Table 4.1: Summary of the exponents for the fitted power functions in Figures 4.3 to 4.7 with scale breaks, where applicable.

Plot	Segment	Scale Break (km)		Exponent			Figure
		First	Second	First	Second	Third	
All variance pairs	all	none	-	0.87	-	-	4.1
One function variogram	all	none	-	1.27	-	-	4.2
Three function variogram	all	100	340	0.034	1.04	3.18	4.3
North-south zones	North	100	-	-0.32	0.93	-	4.4
	South	100	-	0.75	1.74	-	
Land cover types	Crossed	none	-	2.37	-	-	4.5
	Evergreen	100	-	-0.50	1.34	-	
	Non-Evergreen	100	-	0.40	1.19	-	
	Mixed	100	-	0.22	1.96	-	

The daily SWE semi-variance shows variability, but no increase with distance for the last day when all 90 SNOTEL stations were in accumulation from four different snow years (*Figure 4.6*). Each date illustrates the same sequence of variability (increasing or decreasing with lag

distance, but there are no scale breaks for any of the four dates (*Figure 4.6*). Even the distances where the bins had less than 20 station pairs, at the shortest and largest lag distances, showed the same variability among the years (*Figure 4.6*). For the latest date in an accumulation period (03/01/97) the semi-variance is the largest of the four dates on this plot. The amount of SWE affects the magnitude of the semi-variance across the domain (*Figure 4.6*), such that the larger the average SWE across all stations, the larger the semi-variance in SWE. Although the magnitudes of semi-variance differ among the years (*Figure 4.6*), the data follow the same general pattern each year at any given lag distance. These patterns are easier to visualize when the data are standardized (*Figure 4.7*).

Dividing the semi-variance by the square of the mean SWE on four dates during the 1997 accumulation season standardizes the data and illustrates consistent patterns at all lag distances throughout the accumulation season (*Figure 4.7*). These patterns are similar to the different years (*Figure 4.6*) and show an increase in semi-variance up to only 4 km when there are fewer than 20 station pairs. There is both inter-annual consistency (*Figure 4.6*) and intra-annual consistency (*Figure 4.7*) in the spatial accumulation patters.

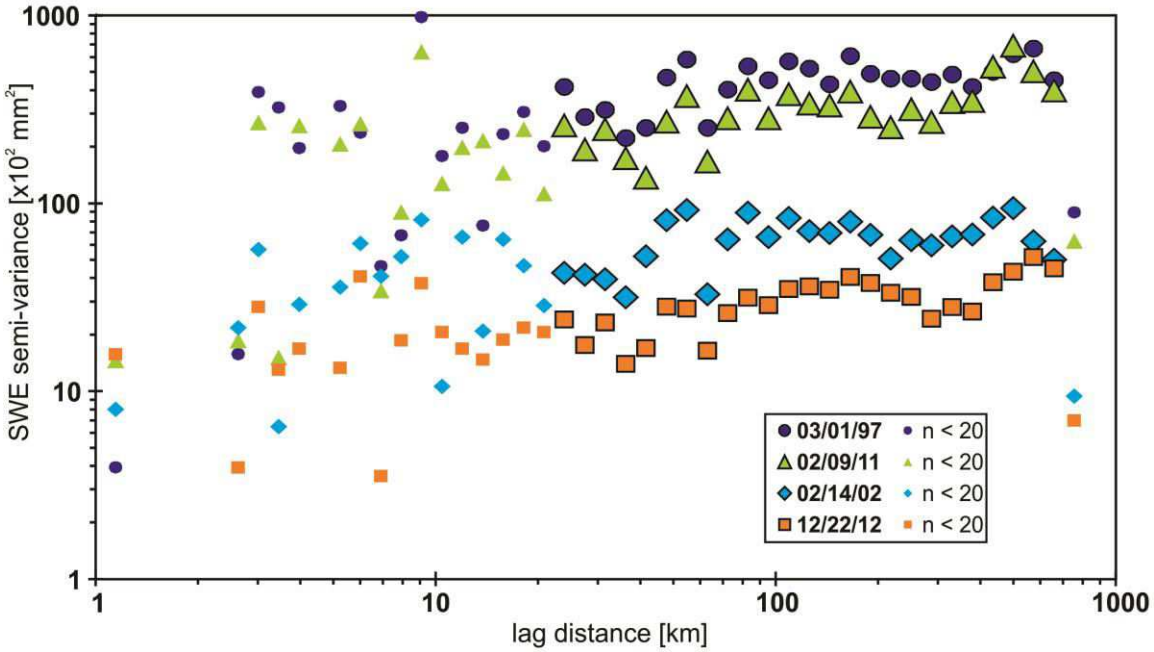

Figure 4.6: Variogram of SWE on the last day all stations are in accumulation for four selected years. The four years represent two low (winter 2013 was the lowest peak annual SWE on record) and two high (winter 1997 was the highest on record) accumulation years. The mean SWE at the last day of accumulation was 99, 180, 366, 532 mm for winters 2013, 2002, 2011, and 1997, respectively. This is for lag distance bins with and without 20 station pairs.

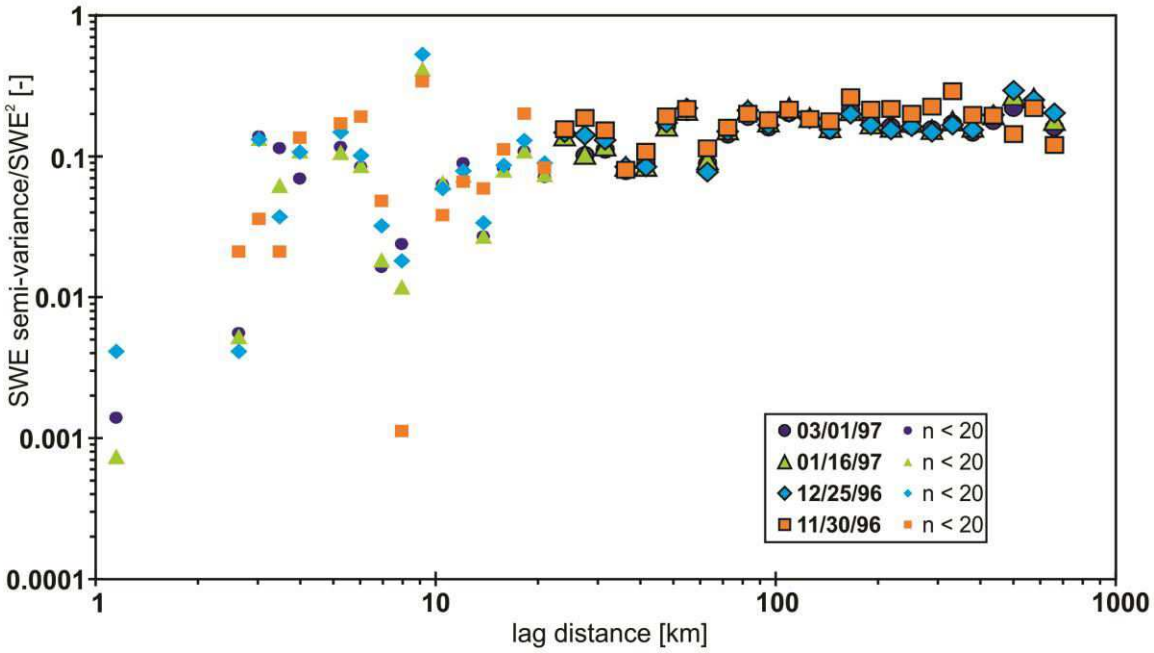

Figure 4.7: Variogram for the four days of accumulation at all stations during the winter of 1997 with and without 20 station pairs per bin. The four dates include the first and last days with accumulation at all stations. Note that the y-axis has been standardized by the square of the mean SWE for the day.

CHAPTER 5:

Discussion

5.1 Scale Breaks and Consistent Patterns

The variogram plots inform the scale of spatial variability for accumulation slopes among all stations. The linear segments of the fitted power functions identify the scales of spatial variability for various lag sections separated by scale breaks (*Figure 4.3*). Initially there is little spatial variability until the first scale break at 100 km (first section in green in *Figure 4.3*). After 100 km there is an abrupt increase in semi-variance (second section in blue in *Figure 4.3*). At approximately 340 km, the semi-variance displays an abrupt increase, warranting another scale break (third section in purple in *Figure 4.3*). The lag distance of such lag sections denote the specific scale of such spatial variability.

The variograms are displayed in log-log space because snow distribution is a complex non-linear system that often displays fractal distributions, and is best characterized by power-law behavior, as is such in many magnitude-frequency relationships (Malamud and Turcotte, 1999). In other words, the semi-variance in accumulation rates increases very quickly at certain lag distances, and to pick out scale breaks the semi-variance data is regressed with power functions and displayed in log-log space, as is consistent with Deems *et al*. (2006). Identifying scale breaks as abrupt increases in the semi-variance is not always clear-cut. Comparing the difference in the exponents of adjacent lag sections is a means of deciding whether a scale break exists or not. For instance, the difference in exponents between the first and second lag sections in *Figure 4.3* is 1.006, and the difference between the second and third lag sections is 2.14.

The metric being assessed in *Figure 4.1* through *Figure 4.5* (semi-variance of relative accumulation rates computed as a slope) is an indirect measure, or a statistical descriptor, not an

actual snow variable such as snow depth or SWE (e.g., *Figure 4.6* and *Figure 4.7*) used by others (e.g., Deems *et al.*, 2006). *Figure 4.1* shows the spread of the semi-variance data in non-binned fashion. *Figure 4.2* is a variogram that averaged the semi-variance data in *Figure 4.1* into 20 km-width bins, and fit a power function through all of the data, without separating lag sections. *Figure 4.3* identifies a short lag section, a medium lag section, and a long lag section. From this information we gather that relative accumulation slopes in the southern Rocky Mountains are similar up until 100 km. From 100 to about 340 km, the relative accumulation slope displays a steeper, but constant, linear increase. Beyond 340 km, the relative accumulation slope shows another steeper increase (*Table 4.1*). It was hypothesized that there would just be one scale break, but two incremental scale breaks exist (*Figure 4.3*). A second scale break helps necessitate examining the accumulation in different zones.

Consistent, in the context of accumulation rates, is defined as the inter/intra-annual value of accumulation slopes adhering to the same general pattern relative to its' surrounding accumulation rates. In the variogram plots (*Figure 4.3* through *Figure 4.5*) the method to determine inter-annual consistency in accumulation patterns is to identify lag sections with relatively constant slope in the semi-variance. Typically, the correlation length relates to the lag sections and is the lag distance beyond which there is no correlation between adjacent points, and only exists for stationary or locally stationary processes (Webster and Oliver, 2001). Although we applied the same method in determining correlation length, snow accumulation is not a locally stationary process; here we see no change in variability until the first scale break and thus no correlation as per the variogram definition (Isaaks and Srivastava, 1989).

5.2 Subset Analysis: Location-Based Station Pairings

The north and south zone station pairs separated (tan and blue data points in *Figure 4.4*, respectively), as well as the remaining crossed zone station pairs (red data points), illustrate difference amongst the two areas. This subset analysis compliments the work from Fassnacht and Derry (2010) in which the scale of variability over this study domain was highlighted to have a north-south divide in snow climatology. Locally, some SNOTEL stations in the Upper Rio Grande had snow climatology characteristics more similar to stations hundreds of miles away in Arizona, than other nearby stations (Fassnacht and Derry, 2010). The station pairs in the north zone in *Figure 4.4* have a slightly larger areal extent than the south zone, and the variance increased less with distance, i.e. less variability in relative accumulation slopes, than the south zone (*Table 4.1*). The crossed station pairs have an initial minimum lag distance of 100 km and a fitted power function that exhibits the steepest increase of the three zones (*Table 4.1*). Variance begins to increase more beyond 100 km in the south zone stations, but the increase is not abrupt enough to warrant a scale break.

For the north zone stations there may be a scale break at 280 km, but this lag distance is at the end of the extent of north zone stations. Such a scale break would be consistent with the second scale break found in the all station pairs variogram (*Figure 4.3*) at 340 km. For the crossed station pairs, there are no discernible scale breaks. Even though the north and south zones exhibit differing slopes in relative accumulation rates, no obvious scale breaks were identified in either zone. This difference in accumulation rates can be attributed to differing climatology in the north and south zones. There are surprisingly few stations around the 38°45'N divide. There is a topographic divide about this parallel, also seen through the distributions of the

stations (*Figure 2.1*). There are no long-term stations in the northern Sangre de Cristo Mountains (above 3000 m in the north-east part of south zone in *Figure 2.1*).

5.3 Subset Analysis: Land Cover-Based Station Pairings

Land cover affects snow distribution (Zakrisson, 1981; Elder *et al.*, 1991; Trujillo *et al.,* 2007; Sexstone and Fassnacht, 2014), and scale breaks are observed at 100 km for each land cover type (*Figure 4.5*). The evergreen pairs have the largest difference in rates of change in variability about the scale break. The mixed pairs have the next largest difference between the variance about the scale break, and the non-evergreen pairs have the smallest difference (*Table 4.1*). While Winkler and Moore (2006) found canopy closure to be one of the most influential controls on accumulation variability, they looked at a much finer scale. A consideration for examining SNOTEL stations in forested areas is the size of the station's footprint, as the stations are always located in small clearings of about 5 to 10 m when installed in dense forests. Such clearings are not always evident in the 30-m land cover data. Furthermore, there are no SNOTEL stations located above tree line in the southern Rocky Mountains (Fassnacht *et al.*, 2012), which is an area with substantial snow accumulation and redistribution that is not well measured. If the difference in exponents of the functions fitted to the relative accumulation slopes were substantially larger for evergreen or in non-evergreen, it would indicate that that particular land cover has an effect on relative accumulation slopes. However, because the difference in exponents was relatively small for all three land cover pairings, land cover was found to have little effect systematic on relative accumulation slopes in the southern Rocky Mountains. The footprint of SNOTEL stations is also a cause for consideration of land cover effects, because less

snow is intercepted above the SNOTEL stations and more snow accumulates on the snow pillow than in the surrounding forest.

The scale breaks at 100 km lag distance for station pairs in all three land cover types (*Figure 4.5*) agrees with the first scale break in *Figure 4.3*. A further sub-analysis was performed by separating station pairs in the north and south zones by land cover type. There are only enough pairs (20 required per bin) for the north zone evergreen combination. The same scale break at 100 km was found in the north evergreen station pairs. The fitted power function has an exponent before the scale break of -0.18, and 0.59 after the scale break, compared to all stations evergreen pairs (*Figure 4.5*) exponents of -0.50 before the scale break, and 1.34 after the scale break.

5.4 Inter/Intra Annual Individual-Day SWE Variability

The individual day SWE variograms (*Figure 4.6* and *Figure 4.7*) show like patterns at similar lag distances on all four dates. For example, in *Figure 4.6* from the 20 km lag distance to 60 km lag distance there is a dip followed by an increase in the SWE semi-variance on all four dates. These patterns are even more apparent in *Figure 4.7*. No scale breaks exist in either of the plots, suggesting that using SWE for a day when all stations are in accumulation cannot be used to define scales of variability. *Figure 4.6* shows that in a particular year the variance in SWE among all 90 stations is correlated to the average SWE for a particular date. The larger the mean SWE for a particular date, the higher the variance. Other studies (e.g., Shook and Gray, 1995; Deems et al., 2006) have used this type of variogram analysis to determine scale breaks, but none were found in *Figure 4.6* nor in *Figure 4.7* in our analysis. Here the distances are much greater than in previous studies and it is likely scale breaks exist at much shorter or longer distances, uch

that the non-correlation part of the variogram was presented in *Figure 4.6* and *Figure 4* (Blöschl, 1999). It is possible that the variogram method is not usable for this range of SWE data.

5.5 Relative Accumulation Slope: High and Low Semi-Variance and Storm Tracks

While the relative accumulation slopes between two stations can be similar for two years, it typically varies from year to year. Different relative accumulation slopes are also seen at varying lag distances (*Figures 4.1* to *4.5*). *Figure 3.2 a* and *c* shows plots of two sets of station pairs; one has very similar accumulation patterns with a short lag distance (*Figure 3.2a* for Niwot and University Camp SNOTEL stations that are 2.7 km apart) and the other pair has differing accumulation patterns and a larger lag distance (*Figure 3.2c* for Tower and Upper San Juan SNOTEL stations that are 340 km apart). For each accumulation year relative accumulation slope can vary drastically over the period of record (*Figure 5.1*) The resulting semi-variance value between Upper San Juan and Tower SNOTEL is relatively high at 0.10, whereas the semi-variance value between Niwot and University Camp SNOTEL is 0.01 (*Figure 3.2a*).

The semi-variance increases with distance due to less similarity in accumulation patterns at larger distances (*Figures 4.3* through *4.7*). The semi-variance value between Tower SNOTEL and Upper San Juan SNOTEL is derived from year-to-year differences (*Figure 5.1*). In accumulation year 2006 (large blue diamonds, *Figure 5.1*) the Tower SNOTEL recorded much more snow accumulation than the Upper San Juan SNOTEL, illustrated by the relative accumulation slope of 0.31. During this same accumulation year the peak SWE during concurrent accumulation at Tower SNOTEL was 1493 mm while the peak SWE at Upper San Juan SNOTEL was 508 mm. Conversely, the snow year 2005 (large purple diamonds, *Figure 5.1*) had the highest relative accumulation slope on record for this SNOTEL pair at 1.85, with the

peak SWE during accumulation at Tower SNOTEL being 983 mm, and the peak SWE at Upper San Juan also being 983 mm. This is an example of how large differences in accumulation years yield large semi-variance values. However, it should be noted that the semi-variance between these two stations (0.10 in *Figure 3.2d*) is an order of magnitude less than the average (about 1.13) from the best fit line(s) for individual points (*Figure 4.3*) or for the average of all stations that are 320 to 340 km apart (*Figure 4.5*). This is likely since both stations have deep snowpacks regardless of the year (*Figure 5.1*).

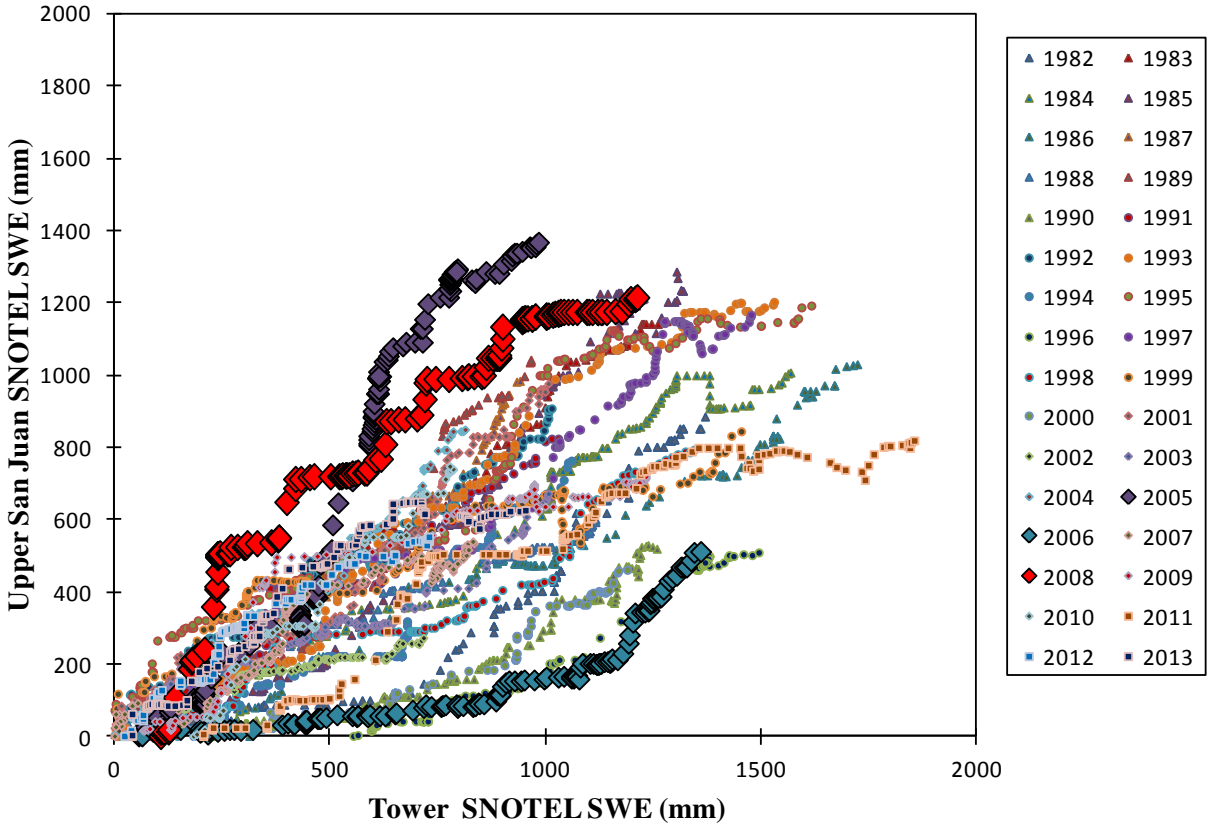

Figure 5.1: Concurrent accumulation slopes for 32 years of record between Upper San Juan SNOTEL and Tower SNOTEL. Snow year 2008 is highlighted by large red data points and shows how differing storm tracks affect these two sites.

The Upper San Juan SNOTEL is in the south zone (south of 38° 45' N) and the Tower SNOTEL is in the north zone, which have differing snow climates (Fassnacht and Derry, 2010). A primary reason for these differing snow climates is storm tracks (Changnon *et al.*, 1991). For

example, snow accumulation year 2008 (large red data points, *Figure 5.1*) shows a step-wise increase through the progression of the particular accumulation year, illustrating how different storm tracks can result in accumulation at one station and not the other. Specifically when a set of data points from 2008 show a vertical progression this indicates that Upper San Juan SNOTEL is accumulating snow and Tower SNOTEL is not, and when the data points show a horizontal progression the Tower SNOTEL is accumulating snow and Upper San Juan SNOTEL is not. Such step-progression in the comparable accumulation does not always occur between the Upper San Juan and Tower SNOTEL stations.

5.6 Bin Requirements and Direction of Scale Breaks

When generating the variograms and fitting the functions, bins with less than 20 SNOTEL pairs were excluded. These points do still appear on the variograms, but they were not used in calculating any of the best-fit curves. Deems *et al.* (2006) used the same approach and did not include these in the variogram calculations (Deems, *pers. comm.*, 2015) in that several bins at the shortest and longest lag distances were considered outliers. All of the excluded bins containing less than 20 pairs per bin in *Figure 4.4 and Figure 4.3* trend towards sharply decreasing semi-variance values with lag distance, which is in disagreement with the semi-variance trends. The bins excluded from the fitted power functions in the variograms are for the most part at the largest and shortest lag distances. Isaaks and Srivastava (1989) recommend changing the bin size to better incorporate all spatial data. However, it is important to choose bin widths that are practical and consistent with the scale being assessed. Furthermore, while this removes data from the variogram calculation, it can make the structure of the variogram clearer.

Traditional variogram analyses at smaller scales find that semi-variance increases with lag distance until a scale break, when the semi-variance stops increasing (e.g. Deems *et al*., 2006). However, across multiple scales there can be steps in the variance (Bloschl, 1999; Deems *et al*., 2008). The direction of change in semi-variance observed about the scale breaks in Deems *et al*., (2006) is from faster increase to slower increase across the scale break, while the direction of change at the scale breaks in this study is from slower increase to faster increase. Bloschl (1999) noted that process interactions that create spatial snow distribution are very complex, and as the scale of interest changes, the observed variability also changes. Such differences in the direction of variance change at scale breaks between Deems *et al.* (2006) and this study can exists for a variety of reasons. The variograms constructed in Deems *et al.* (2006) were from direct measurements of snow using a continuous dataset (lidar remote sensing), while the variograms presented herein are a product of accumulation patterns measured at a point, and are a statistical summary of the comparison of station data. The variograms in Deems *et al.* (2006) had a spatial extent of roughly 1.2 km and were at the measurement scale, while the extent of this study is 757 km and is at the modeling scale. The support and spacing of the Deems *et al.* (2006) data were the same at about 1.5 m, while in this study the support is 6 m, and the spacing is at least 2.7 km. The scale of interest can affect the variability in spatial trends, such that if the spacing between stations is too large then the small scale variability will not be appropriately represented, and conversely if the station spacing is too small then the large scale variability will not be represented (Bloschl, 1999). Additionally, if the support is too large the data will be smoothed resulting in the variability being smoothed. Most previous snow distribution studies examined much smaller domains. The resolution of the variogram in Deems *et al.* (2006) is much finer, the scale is smaller, and the scale breaks in snow depth occur at 15 to about 40 m

across three different sites. The scale breaks in SWE in this study (*Figure 4.3* and *Figure 4.5*) occur at 100 km, 140 km, and 340 km across the entire domain. There are different driving forces on distribution at these varying scales. At the measurement scale the primary driving forces, are wind, vegetation, topography, and slope, while the primary driving force for accumulation at the modeling scale in this study is likely the storm track.

5.7 Analyzing Accumulation Season Instead of Melt Season

The accumulation period was the primary focus of this study and the melt period was disregarded for several reasons. The number of days with concurrent melt between station pairs is much fewer than the number of days of concurrent accumulation over the period of record. This occurs since there are often lower elevation SNOTEL stations that have melted out, i.e., no snow, while other higher elevation stations have a substantial snowpack and may still be accumulating. Process changes in snowpack properties occur with the transition from the accumulation to the melt season. Constructing a variogram across the periods of accumulation and into melt spans these process changes. These are different processes and different variability is seen when stations/locations are in different phases (Egli and Jonas, 2009).

5.8 Precipitation Patterns through Entire Winter Season and Summer Season

A simple correlation plot was made to see how accumulation patterns compare to entire winter precipitation, as well as among winter precipitation and summer precipitation using data from the 90 long-term SNOTEL stations (*Figure A8 in Appendix*). There is a good correlation ($R^2 = 0.96$) between accumulation semi-variance and winter precipitation semi-variance. The correlation between winter precipitation semi-variance and summer precipitation semi-variance

($R^2 = 0.51$) is not as good. *Figure 5.2* displays is a scale break in the winter precipitation between 280 and 350 km, which is consistent with the second scale break in *Figure 4.3,* and the summer precipitation shows a scale break at a shorter lag distance, between 60 and 140 km. *Figure A8* shows that the accumulation patterns observed in *Figure 4.1* through *Figure 4.5* are consistent through the winter season, and vary during the summer season.

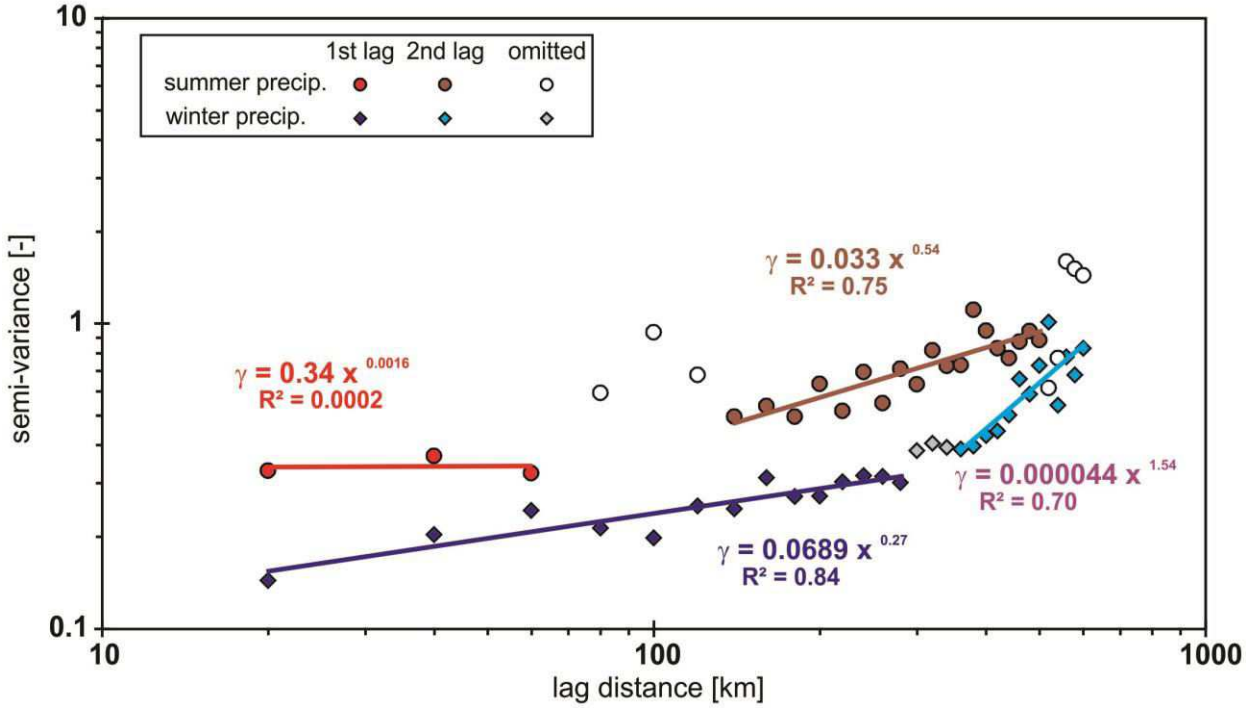

Figure 5.2: Variogram of winter precipitation (accumulation and melt phase in blue data points) and summer precipitation (red and brown data points) from period of record.

5.9 Data Limitations

While the data obtained from the NRCS SNOTEL network have undergone quality assurance and quality control, such data are not completely indicative of true conditions. For instance, Bloschl (1999) elaborated on how instrument error and the spatial dimensions of the instruments at SNOTEL stations cause error. Further, the patterns and statistical moments of the data will be different from the true patterns and statistical moments. While the SNOTEL network

does represent the temporal variability of SWE, it poorly represents the spatial variability of SWE, particularly in mountainous watersheds (Fassnacht *et al*., 2012; 2016). SNOTEL stations are known to not represent their surrounding areas (Kashipazha, 2012; Merormy *et al.,* 2013) but they are indices that are representative of themselves (Fassnacht *et al.,* 2012; Sexstone and Fassnacht, 2014). Location attributes of SNOTEL stations in the southern Rocky Mountains are somewhat homogeneous with relatively flat slope and open canopy near tree line (Sexstone and Fassnacht, 2014), and different periods during the snow season (accumulation and sublimation) are better represented by some SNOTEL locations than others. For example, if the forest surrounding a SNOTEL is patchy with regular-spaced clearings, the SNOTEL station will likely better represent the actual accumulation of surrounding conditions compared to a SNOTEL station that is surrounded by thick evergreen forest. There are large gaps in the spatial coverage of the study domain in areas of persistent snow (*Figure 2.1*), particularly around and south of the dividing parallel (38° 45'N). Molotch and Bales (2005) found that on average less than 2.4% of surrounding grid elements were optimally represented by its' SNOTEL location attributes during the accumulation season. This means that variability in accumulation should be expected along the distance between adjacent SNOTEL stations and that measured accumulation provides a rough estimate of the relative magnitude of snow accumulation surrounding a SNOTEL. Overall, the SNOTEL network has the best spatial coverage of SWE within the study region and the SNOTEL data were the best option for analyzing spatial and temporal trends and patterns across the study domain.

Snow accumulation increases with elevation (Washichak and McAndrew, 1967; Dingman, 1981) due to orographic effects (Doesken and Judson, 1996). Elevation is thus the variable that has the strongest correlation with peak SWE (Fassnacht *et al*., 2003). All SNOTEL

stations are in areas of persistent snow (Richer *et al.*, 2013; Moore *et al.*, 2014), so adjacent stations at different elevations will both receive snow around the same time. As seen from *Figure 2.2,* elevation of the SNOTEL stations used in this study poorly represents the actual elevations within the maximum snow-covered extent in the southern Rocky Mountains (Fassnacht *et al.,* 2012). As such, the station pairs were not subset (e.g., north versus south or by land cover) to consider elevation bands.

CHAPTER 6:

Conclusion

The premise of this study is that there exists a physical distance at which snow accumulation patterns across the southern Rocky Mountains vary abruptly. Variogram analysis used data from 90 long-term SNOTEL stations to determine if such a physical distance exists. It was found that the relative accumulation among all 90 SNOTEL stations in the southern Rocky Mountains is similar up until a physical distance of about 100 km. From 100 to 340 km the relative accumulation rate displays a steeper, but constant, almost linear increase. Beyond 340 km, the relative accumulation rate shows a much steeper increase. It was hypothesized that there would be a scale break in the relative accumulation slopes; two scale breaks were observed showing that relative accumulation slopes exhibit fractal characteristics. A plot of semi-variance in relative accumulation slope versus lag distance for all 4005 station pairs exhibited an increase with lag distance, but also a large spread in the variance indicating that factors other than just distance influence the relative accumulation between stations.

One variogram was computed from daily SWE values from the last day when all 90 stations were in accumulation for the following four winters: 1997, 2002, 2011, and 2013, representing a high accumulation year, two average accumulation years, and a low accumulation year, respectively. A second variograms was computed from four individual dates during the 1997 accumulation season, representing the first and last day when all stations were accumulating, and two mid accumulation dates. These variograms showed that the semi-variance was a function of SWE and similar undulating patterns for specific lag distances were observed on all four dates in both inter- and intra-annual cases, illustrating patterns exist at similar lag

distances. However, no scale breaks were found in either of the variograms, so scales of variability could not be defined from the individual-day SWE data.

Two subsets divided stations based on their north-south position, and based on their land cover type. The north-south position subset utilized a variogram that split the study region in half at the latitude line 38°45'N, creating separate results for a north zone, a south zone, and across the zones (crossed). The relative accumulation slope was steeper in south zone than in the north. The difference in relative accumulation slopes is due to differing climatology and storm tracks in the north and south zones. Scale breaks were found in the north and south zones at 100 km and are in agreement with the first scale break found in the all stations variogram.

The second subset divided stations by land cover into three groups: evergreen, non-evergreen, and mixed. Scale breaks were detected at 100 km for each land cover type and the difference in exponents about the scale breaks of the fitted power functions were considered. The evergreen pairs had the largest difference in exponents about the scale break (difference of 1.84), the mixed pairs had the next largest difference (1.74), and the non-evergreen pairs had the smallest difference in exponents (0.79). Had the difference in exponents been substantially larger for the evergreen or non-evergreen pairing it would have indicated that that particular land cover had an effect on relative accumulation slopes. From these findings, land cover was found to have little effect on relative accumulation slopes in the southern Rocky Mountains.

CHAPTER 7:

Recommendations

The results shown herein could help identify where additional stations should be established to extend station coverage and fill in gaps of snow data collection: From any given SNOTEL station, the largest spacing to the next closest SNOTEL station in all four cardinal directions should be no greater than 100 km, within reasonable means. Additional evaluation of the existing dataset could increase station coverage to better represent actual elevation ranges within the study region. For example, stations could be sub-divided into elevation zones for further variogram analysis to examine elevation-based spatial patterns in accumulation. Additionally, seasonal and inter-annual variability in synoptic weather patterns could be considered to divide SNOTEL station pairings. Further sub-setting of station pairs could be based on land cover types within each of the defined north and south zones to better understand the scale breaks. Currently there are 145 operational SNOTEL stations in the southern Rocky Mountains; in the future with a longer period of record for the newer station, the analysis presented here could be updated to evaluate changes in accumulation patterns.

The methods presented herein could be applied to examine accumulation patterns across other domains, such as other parts of the Western United States where SNOTEL stations are operated or other countries will a similar network of automated or high temporal resolution monitoring. The methods could also be applied to other similar variables, such as seasonal cumulative precipitation, or cumulative snowmelt rates.

The variogram analysis using the variance of the relative accumulation slope is but one statistical approach. Future consideration could also be given to how well a linear regression fits each years' relative accumulation slope using different statistics, such as the coefficient of

determination (R^2). For example, the close proximity University Camp and Niwot SNOTEL station pair would exhibit strong correlation each year, as presented by a high R^2 value. Conversely, linear regression fits between the further-spaced Upper San Juan SNOTEL and Tower SNOTEL would yield smaller R^2 values, illustrating accumulation is less well correlated between these two stations. This approach could be used in a manner to rank the station pairs on how consistent accumulation patterns are among station pairs, and also be paired with storm track characteristics to explore their affect on accumulation patterns.

LITERATURE CITED

Abatzoglou, J. T., D. E. Rupp, and P. W. Mote, (2014). Seasonal Climate Variability and Change in the Pacific Northwest of the United States. *Journal of Climate,* **26**(5) 2125-2142, DOI:10.1175/JCLI-D-13-00218.1

Anderton, S. P., S. M. White, and B. Alvera (2002). Micro-scale spatial variability and the timing of snow melt runoff in a high mountain catchment, *Journal of Hydrology*, **268** (1–4), 158–176, DOI: 10.1016/S0022-1694(02)00179-8.

Bales, R. C., Molotch, N. P., Painter, T. H., Dettinger, M. D., Rice, R., and J. Dozier, (2006). Mountain hydrology of the western United States, *Water Resources Research*, **42**, W08432, DOI: 10.1029/2005WR004387.

Barry, R. G. (2008). Mountain Weather and Climate, 3rd Edition, *Cambridge University Press,* Cambridge. ISBN: 9780521681582.

Blöschl, G., (1999). Scaling issues in snow hydrology, *Hydrologic Processes*, **13**, 2149-2175. DOI: 10.1002/(SICI)10099-1085(199910)13:14/15<2149::AID-HYP847>3.0.CO;2-8.

Brown, R.D., and D. A. Robinson, (2011). Northern Hemisphere spring snow cover variability and change over 1922-2010 including an assessment of uncertainty. *The Cryosphere,* **5**, 219-229, DOI: 10.5194/tc-5-219-2011.

Cayan, D. R., (1996). Interannual climate variability and snowpack in the western United States, *Journal of Climatology,* **9**, 928-947, DOI: 10.1175/1520-0442(1996)009<0928:ICVASI>2.0.CO;2.

Changnon, D., McKee, T. B. and N. J. Doesken, (1991). Hydroclimate variability in the Rocky Mountains, *Water Resources Bulletin,* **27,** 733-743, DOI: 10.1111/j.1752-1688.1991.tb01471.x.

Deems, J. S., Fassnacht, S. R. and K. J. Elder, (2006). Fractal distribution of snow depth from lidar data. *Journal of Hydrometeorology*, **7**, 285-297, DOI: 10.1175/JHM487.1.

Deems, J. S., Fassnacht, S. R. and K. J. Elder, (2008), Interannual Consistency in Fractal Snow Depth Patterns at Two Colorado Mountain Sites, *Journal of Hydrometeorology, Cold Land Processes Experiment Special Collection*, 977-988, DOI: 10.1175/2008JHM901.1.

Dingman, S. L., (1981). Elevation: A major influence on the hydrology of New Hampshire and Vermont, USA, *Hydrology Science Bulletin*, **26**, 399-413, DOI: 10.1080/02626668109490904.

Doesken, N. J. and A. Judson, (1996). The Snow Booklet: A Guide to the Science, Climatology, and Measurement of Snow in the United States, Dep. Of Atmos. Sci., Colorado State University, Fort Collins, CO.

Egli, L. and T. Jonas, (2009). Hysteretic dynamics of seasonal snow depth distribution in the Swiss Alps, *Geophysical Research Letters,* **36**(2), DOI: 10.1029/2008GL035545.

Elder, K., J. Dozier, and J. Michaelsen, (1991). Snow accumulation and distribution in an alpine watershed, *Water Resources Research*, **27**, 1541-1552, DOI: 10.1029/91WR00506.

Fassnacht, S. R., K. A. Dressler, and R. C. Bales, (2003). Snow water equivalent interpolation for the Colorado River Basin from snow telemetry (SNOTEL) data, *Water Resources Research*, **39**, 1208-1218, DOI: 10.1029/2002WR001512.

Fassnacht, S. R. and J. E. Derry, (2010). Defining similar regions of snow in the Colorado River Basin using self-organizing maps. *Water Resources Research,* **46,** W04507 DOI:10.1029/2009WR007835.

Fassnacht, S. R., K. A. Dressler, D. M. Hulstrand, R. C. Bales, and G. Patterson, (2012). Temporal inconsistencies in coarse-scale snow water equivalent patterns: Colorado River Basin snow telemetry-topography regressions. *Pirineos Revista de Ecologia de Montana.* **167,** 167-186. DOI: 10.3989/Pirineos.2011.166008

Fassnacht, S. R., and R. M. Records, (2015). Large Snowmelt versus Rainfall Events in the Mountains. *Journal of Geophysical Research – Atmospheres*, **120,** 2375-2381, DOI: 10.1002/2014JD022753.

Fassnacht S. R., G. Sexstone, A. Kashipazha, I. Lopez-Moreno, M. Jasinski, S. Kampf, and B. Von Thaden, (2016). Deriving Snow-cover Depletion Curves for Different Spatial Scales from Remote Sensing and Snow Telemetry Data, *Hydrological Processes,* HYP-15-0523.R1.

Golding, D. L. and R. H. Swanson, (1986). Snow Distribution Patterns in Clearings and Adjacent Forest. *Water Resources Research*, 22, 1931-1940, DOI: 10.1029/WR022I013P01931.

Hall, D. K., (1988). Assessment of polar climate change using satellite technology. *Reviews of Geophysics*, **26**, 26-39, DOI: 10.1029/RG026I001P00026.

Homer, C. G., Dewitz, J. A., Yang, L., Jin, S., Danielson, P., Xian, G., Coulston, J., Herold, N. D., and K. Megown, (2015). Completion of the 2011 National Land Cover Database for the conterminous United States-Representing a decade of land cover change information. *Photogrammetric Engineering and Remote Sensing*. **77**(8): 758-762.

Isaaks, E. H., and R. M. Srivastava, (1989). An Introduction to Applied Geostatistics. *Oxford University Press, Inc.,* New York, New York, United States of America. ISBN: 9780195050134

Jansa, J., G. Blöschl, R. Kirnbauer, K. Kraus, and G. Kuschnig, (2002). Schneemonitoringmittels Fernerkundung, in Fernerkundung und GIS. Neue Sensoren—Innovative Methoden, edited by T. Blaschke, pp. 241–250, Herbert Wichmann, Heidelberg, Germany.

Kashipazha, A., (2012). Thesis: Practical snow depth sampling around six snow telemetry (SNOTEL) stations in Colorado and Wyoming, United States, Department of Ecosystem Science and Sustainability, Colorado State University.

Kane, D. L, Hinzman, L. D., Benson, C. S. and G. E. Liston, (1991). Snow hydrology of a headwater Arctic basin. 1. Physical measurements and process studies. *Water Resources Research*, **27**, 199-1109, DOI: 10.1029/91WR00262.

Konig, M. and M. Sturm, (1998). Mapping snow distribution in the Alaskan Arctic using aerial photography and topographic relationships. *Water Resources Research*, **34**, 3471-3483, DOI: 10.1029/98WR02514.

Malamud, B. D., and D. L. Turcotte, (1999). Self-organized criticality applied to natural hazards. *Natural Hazards*, **20**, 93–116,

Male, D. H. and D. M. Gray, (1981). Snowcover ablation and runoff. *Handbook of Snow, Principles, Processes, Management and Use*, D. M. Gray and Male, Eds., Pergamon, Press, 360-436.

Martinec, J. and A. Rango (1986). Parameter values for snowmelt runoff modeling. *Journal of Hydrology*, **84**, 197-219, DOI: 10.1016/0022-1694(86)90123-X.

Molotch, N. P., and R. C. Bales, (2005). Scaling snow observations from the point to the grid element: Implications for observation network design. *Water Resources Research.* DOI: 10.1029/2005WR004229.

Molotch, N. P., (2009). Reconstructing snow water equivalent in the Rio Grande headwaters using remotely sensed snow cover data and a spatially distributed snowmelt model. *Hydrological Processes,* **23**(**7**): 1076-1089. DOI: 10.1002/HYP.7206

Molotch, N. P., and L. Meromy, (2014). Physiographic and climatic controls on snow cover persistence in the Sierra Nevada Mountains, *Hydrologic Processes*, **28**(16), 4573-4586, DOI: 10.1002/HYP10254.

Moore, C., S. Kampf, B. Stone, and E. Richer, (2014). A GIS-based method for defining snow zones: application to the western United States. *Geocarto International*, **30,** 62-81, DOI: 10.1080/10106049.2014.885089.

Oliver, M. A., and R. Webster, (1986). Semi-variograms for modeling the spatial pattern of landform and soil properties. *Earth Surface Processes and Landform.* **11**, 491-504. DOI: 10.1002/ESP.3290110504.

Richer, E. E., S. K. Kampf, S. R. Fassnacht, and C. C. Moore, (2013). Spatiotemporal index for analyzing controls on snow climatology: application in the Colorado Front Range. *Physical Geography,* **34,** 85-107. DOI: 10.108/02723646.2013.787578.

Serreze, M. C., M. P. Clark, R. L Armstrong, D. A. McGinnis, and R. S. Pulwarty, (1999). Characteristics of the Western U.S. Snowpack from SNOTEL data. *Water Resources Research,* **35**, 2145-2160, DOI: 10.1029/1999WR900090.

Serreze, M. C., Clark, M. P. and A. Frei, (2001). Characteristics of large snowfall events in the montane western United States as examined using snowpack telemetry (SNOTEL) data, *WaterResources Research,* **37**, 675-688, DOI: 10.1029/2000WR900307.

Sexstone, G. A. and S. R. Fassnacht, (2014). What drives basin scale spatial variability of snowpack properties in northern Colorado? *The Cryosphere*, **8**, 329-344, DOI: 10.5194/TC-8-329-2014.

Shook, K. and D. M. Gray, (1996). Small-scale spatial structure of shallow snowcovers. *Hydrologic Processes*, **10**, 1283-1292, DOI: 10.1002/(SICI)1099-1085(199610)10:10<1283::AID-HYP460>3.0.CO;2-M.

Sturm, M., & A. M. Wagner, (2010). Using repeated patterns in snow distribution modeling: An Arctic example. *Water Resources Research*, **46**: W12549, DOI:10.1029/2010WR009434.

Sturm, M., B. Taras, G. E. Liston, C. Derksen, T Jonas, and J Lea (2010). Estimating Snow Water Equivalent Using Snow Depth Data and Climate Classes. *Journal of Hydrometeorology,* **11,** 1380-1394, DOI: 10.1175/2010JHM1202.1.

Trujillo, E., J. A. Ramirez, and K. J. Elder, (2007). Topographic, meteorologic, and canopy controls on the scaling characteristics of the spatial distribution of snow depth fields.*Water Resources Research.* **43**: W07409. DOI: 10.1029/2006 WR005317.

U.S. Army Corps of Engineers, (1956). Snow Hydrology, Summary Report of the Snow Investigations. U.S. Government Printing Office, 433 pp.

Washickak, J. N. and D. W. McAndrew, (1967). Snow Measurement Accuracy in High Density Snow Course Network in Colorado, Proceedings of the 35th Western Snow Conference, Boise, Idaho, USA, April, 1967.

Webster, R., and M. Oliver, (2001). Geostatistics for Environmental Scientists: Statistics in Practice. *John Wiley and Sons*, 271 pp.

Winkler, R. D., and R. D. Moore, (2006). Variability in snow accumulation patterns within forest stands on the interior plateau of British Columbia, Canada. *Hydrological Processes.* **20**, 3683-3695. DOI: 10.1002/HYP.6382

WMO, (1986). Intercomparison of models of snowmelt runoff. World Meteorological Organization, *Operational Hydrology Report,* **23**, WMO 646.

Zakrisson, K., (1981). Snow Assessments and Snow Distribution in the Malmagen Area at 62°N in Sweden, with Special Reference to Spring Runoff Forecasts. *Physical Geography*, **63**, 11-17, DOI: 10.2307/520559.

APPENDIX A

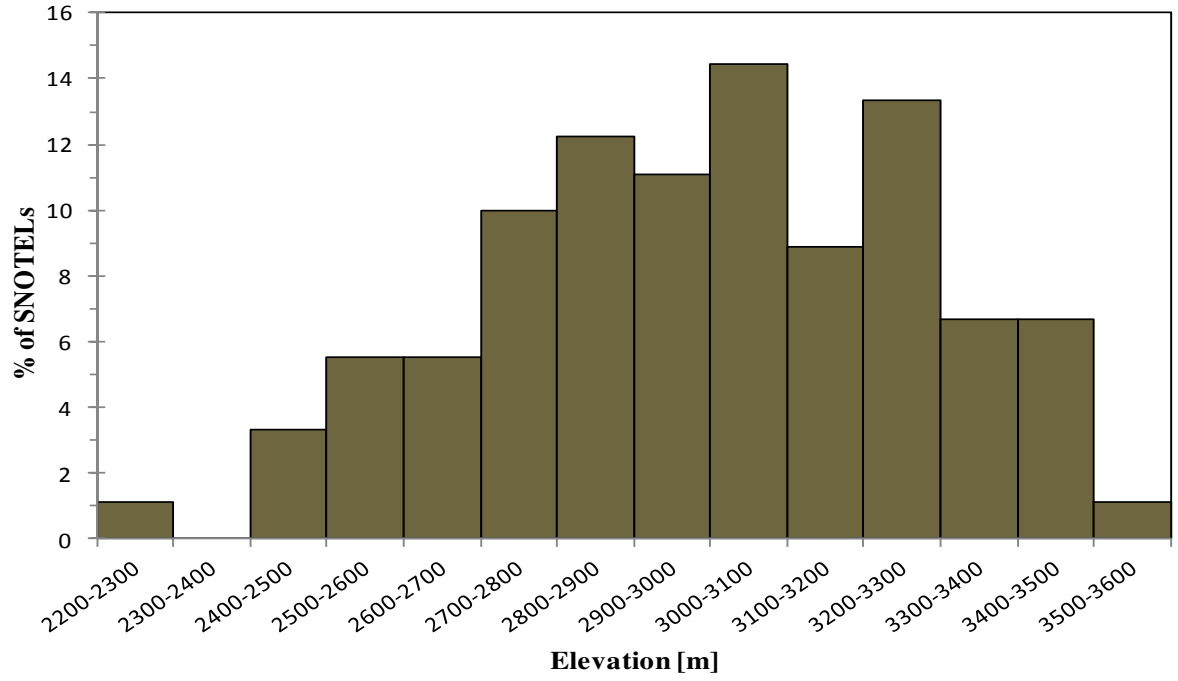

Figure A1: Histogram of elevation for all 90 SNOTEL stations used in the analysis.

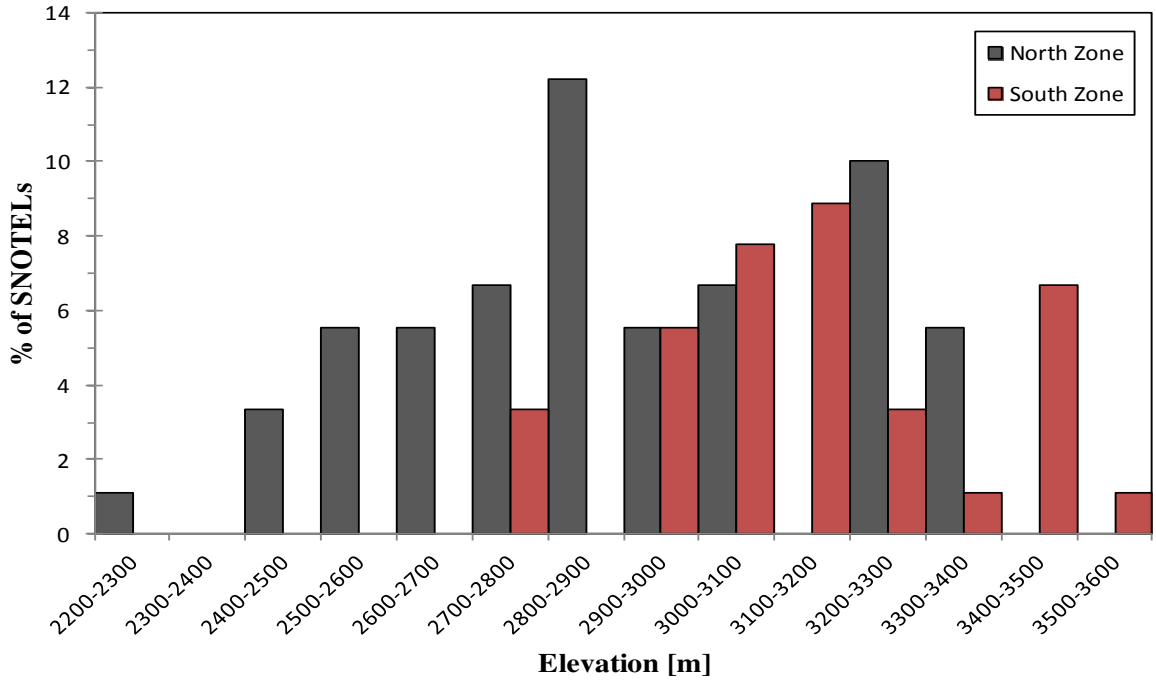

Figure A2: Histogram of elevation for all 90 SNOTEL stations, divided into North and South Zones at the parallel 38°45'N.

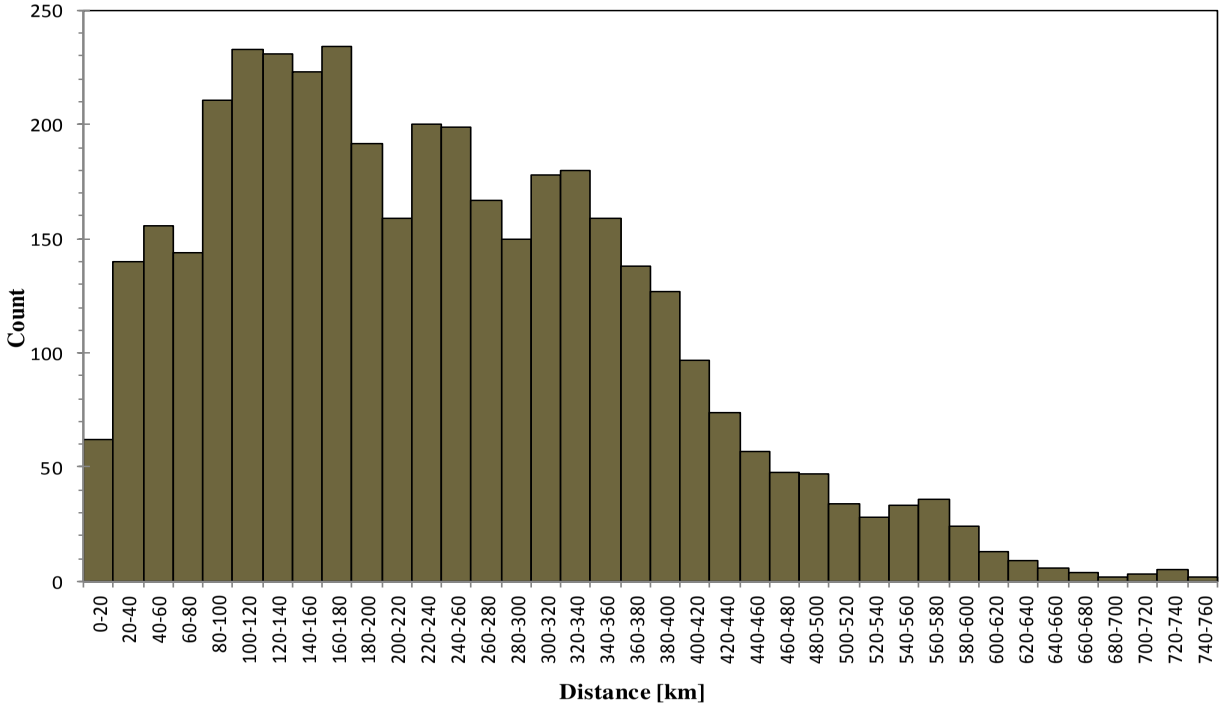

Figure A3: Histogram of distance between all SNOTEL pair combinations in the southern Rockies.

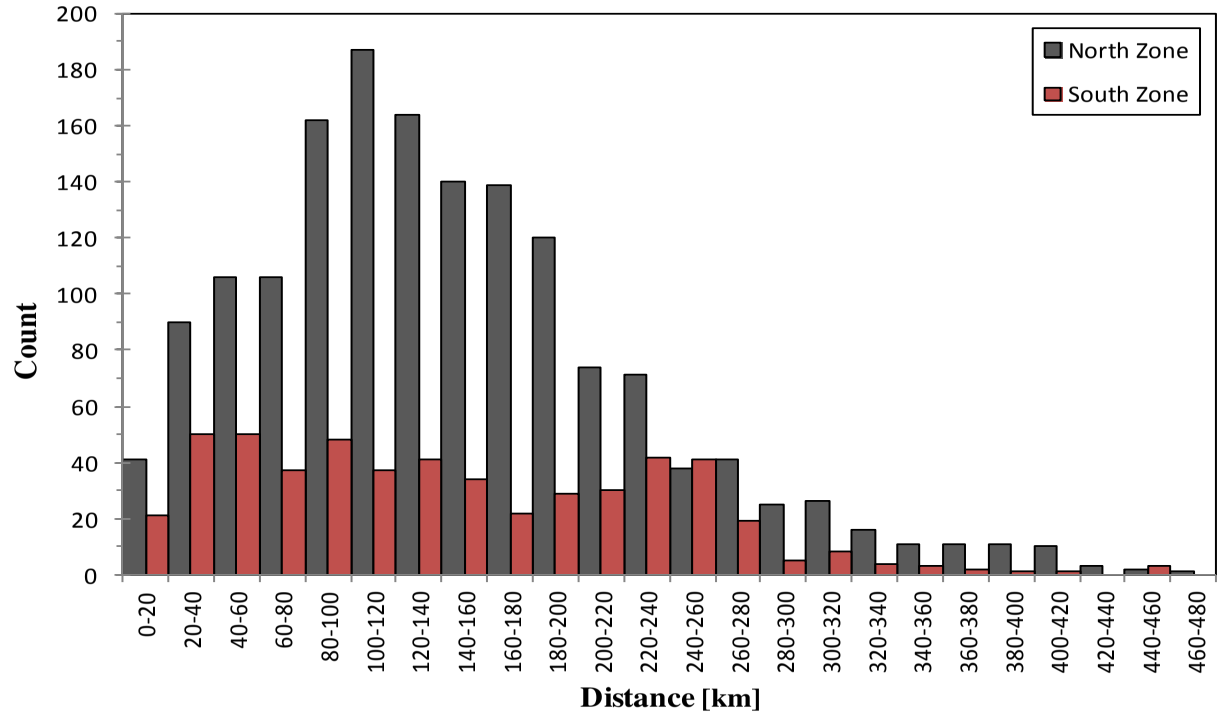

Figure A4: Histogram of distance between SNOTEL pairs, divided into North and South Zones at the parallel 38°45'N.

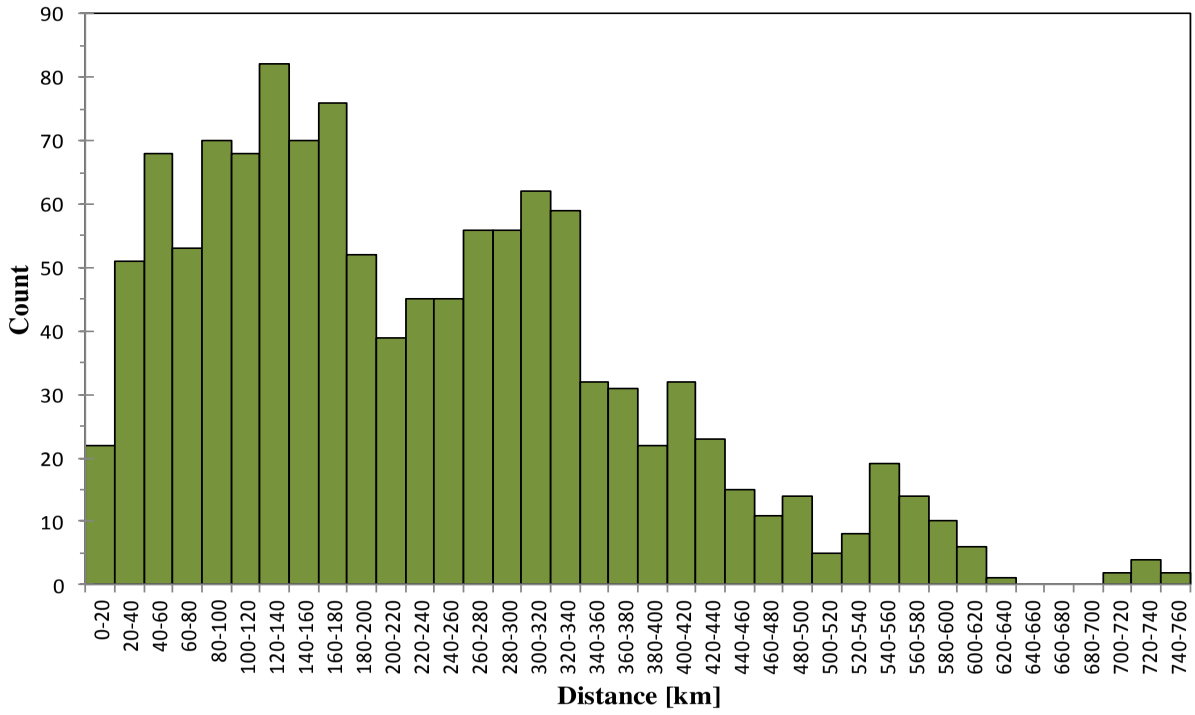

Figure A5: Histogram of distances between all SNOTEL pairs that are in the evergreen land cover type.

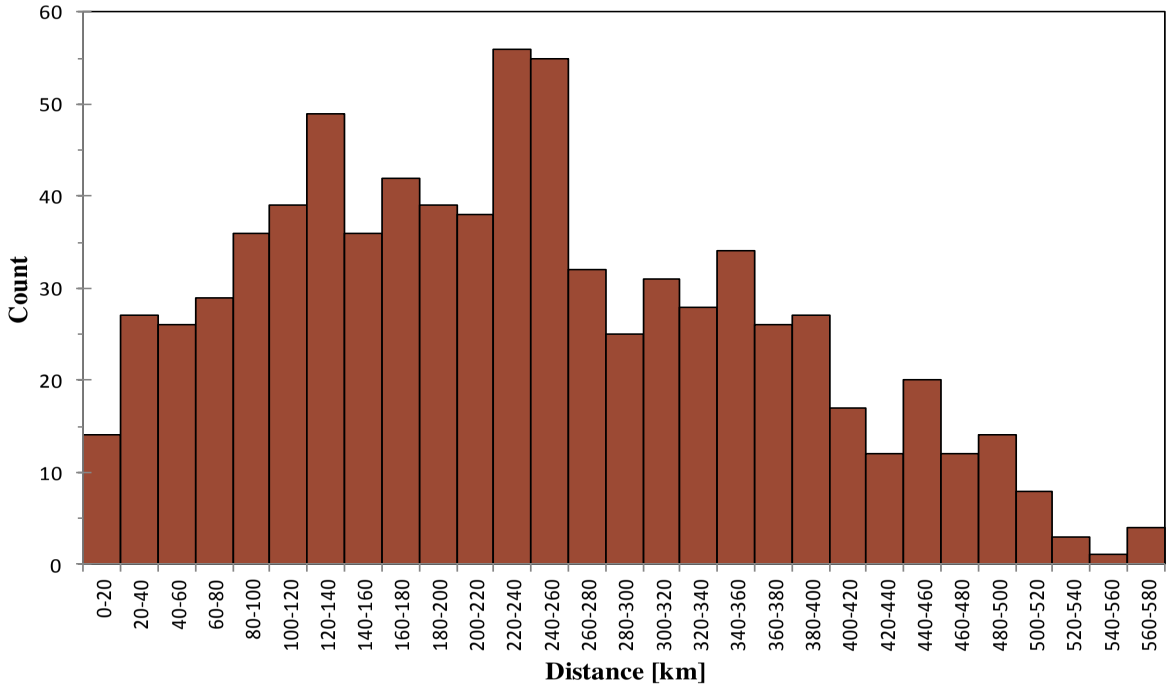

Figure A6: Histogram of distances between all SNOTEL pairs where neither are in the evergreen land cover type.

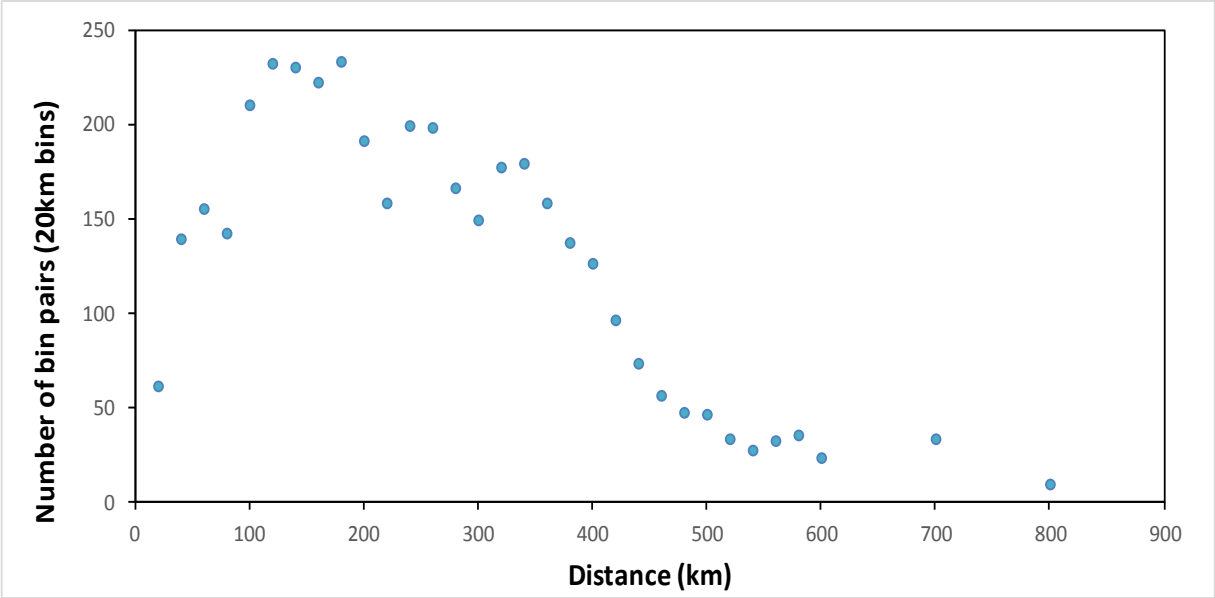

Figure A7: Number of SNOTEL station pairs per 20 km-width bin.

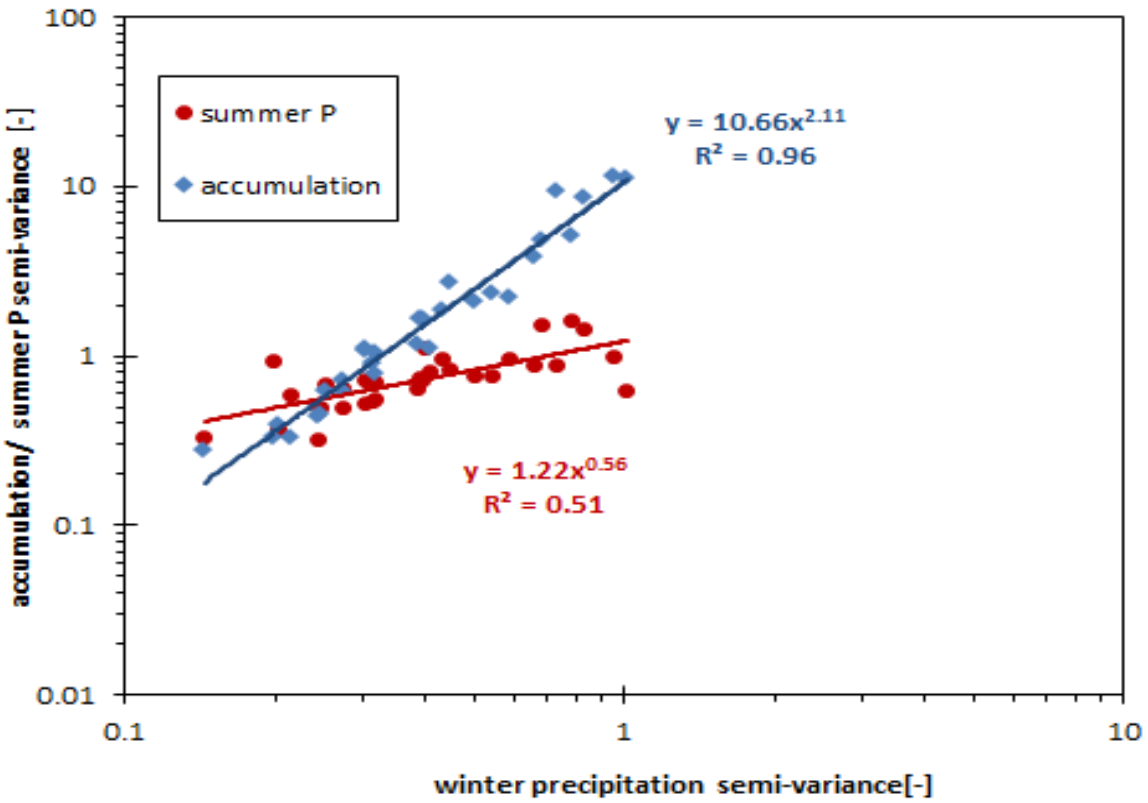

Figure A8: Correlation plot comparing accumulation semi-variance versus winter precipitation semi-variance (blue data points), and summer precipitation semi-variance versus winter precipitation semi-variance (red data points).

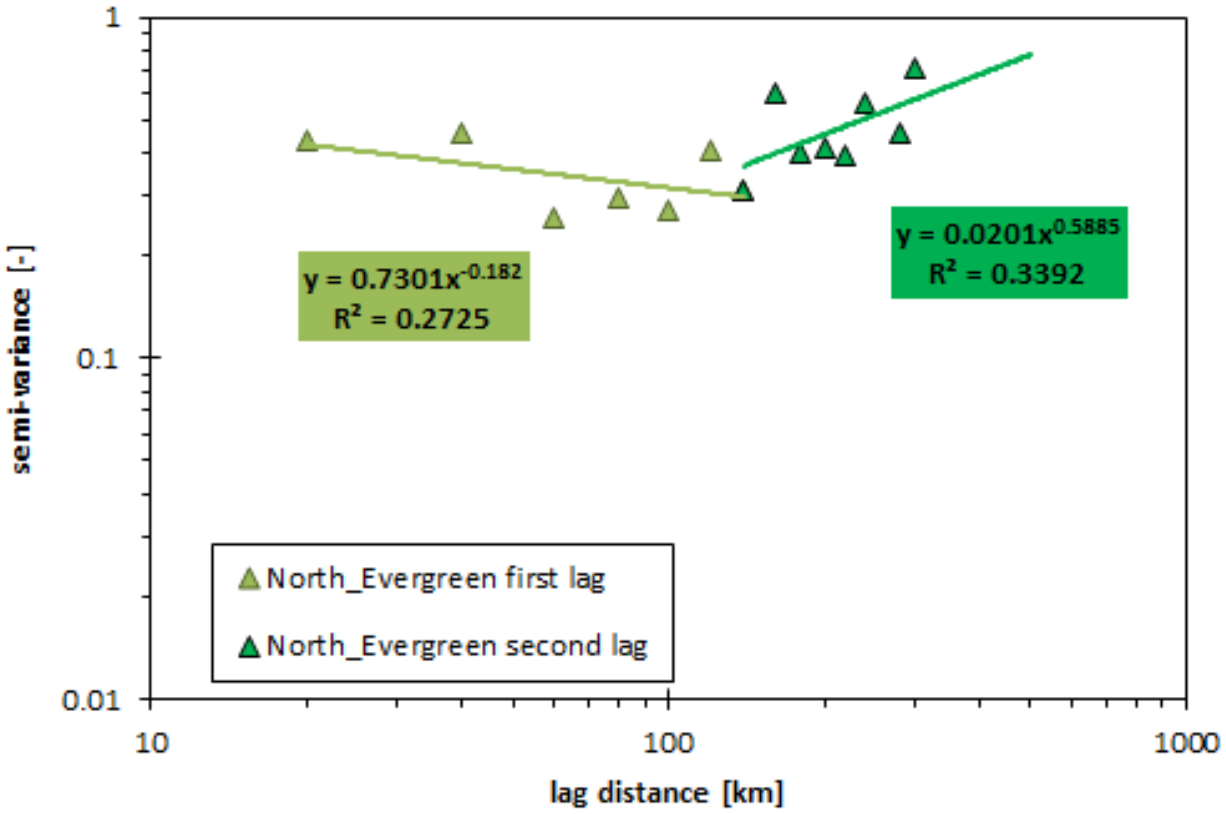

Figure A8: Variogram of north zone evergreen accumulation semi-variance that contain greater than or equal to 20 station pairs. The north zone evergreen was the only subset of pairings that met the 20+ station pairs per bin requirement for the location/land cover subset pairings, with ample data bins to warrant a scale break.

Table A1: The 90 long-term SNOTEL stations and their attributes used herein.

SNOTEL NAME	ELEVATION	LAND COVER	ZONE
PHANTOM VALLEY	2752	Developed, Open Space	North
DEADMAN HILL	3115	Evergreen Forest	North
UNIVERSITY CAMP	3139	Evergreen Forest	North
LAKE IRENE	3261	Evergreen Forest	North
STILLWATER CREEK	2658	Evergreen Forest	North
COPELAND LAKE	2621	Evergreen Forest	North
JOE WRIGHT	3085	Evergreen Forest	North
BEAR LAKE	2896	Evergreen Forest	North
WILLOW PARK	3261	Evergreen Forest	North
LAKE ELDORA	2957	Evergreen Forest	North
NIWOT	3021	Evergreen Forest	North
ARROW	2950	Evergreen Forest	North
GRIZZLY PEAK	3383	Evergreen Forest	North
BERTHOUD SUMMIT	3444	Evergreen Forest	North
CULEBRA #2	3200	Evergreen Forest	South
APISHAPA	3048	Mixed Forest	South
WHISKEY CK	3115	Mixed Forest	South
DRY LAKE	2560	Grassland/Herbaceous	North
COLUMBINE	2792	Evergreen Forest	North
WILLOW CREEK PASS	2908	Evergreen Forest	North
LYNX PASS	2707	Evergreen Forest	North
RABBIT EARS	2865	Evergreen Forest	North
ROACH	2957	Evergreen Forest	North
ELK RIVER	2652	Deciduous Forest	North
TOWER	3200	Woody Wetlands	North
HOOSIER PASS	3475	Evergreen Forest	North
INDEPENDENCE PASS	3231	Grassland/Herbaceous	North
NAST LAKE	2652	Evergreen Forest	North
FREMONT PASS	3475	Grassland/Herbaceous	North
SUMMIT RANCH	2865	Evergreen Forest	North
COPPER MOUNTAIN	3200	Grassland/Herbaceous	North
KILN	2926	Evergreen Forest	North
VAIL MOUNTAIN	3139	Grassland/Herbaceous	North
BRUMLEY	3231	Developed, Open Space	North
PARK CONE	2926	Evergreen Forest	North
PORPHYRY CREEK	3280	Evergreen Forest	South
BUTTE	3097	Evergreen Forest	North

UPPER SAN JUAN	3088	Deciduous Forest	South
WOLF CREEK SUMMIT	3353	Evergreen Forest	South
CUMBRES TRESTLE	3054	Developed, Open Space	South
LILY POND	3353	Evergreen Forest	South
CROSHO	2774	Deciduous Forest	North
RIPPLE CREEK	3152	Evergreen Forest	North
NORTH LOST TRAIL	2804	Mixed Forest	North
BURRO MOUNTAIN	2865	Deciduous Forest	North
PARK RESERVOIR	3036	Grassland/Herbaceous	North
MC CLURE PASS	2896	Deciduous Forest	North
SCHOFIELD PASS	3261	Evergreen Forest	North
BISON LAKE	3316	Grassland/Herbaceous	North
TRAPPER LAKE	2957	Evergreen Forest	North
CASCADE	2707	Deciduous Forest	South
SPUD MOUNTAIN	3249	Developed, Low Intensity	South
MOLAS LAKE	3200	Evergreen Forest	South
MINERAL CREEK	3060	Evergreen Forest	South
UPPER RIO GRANDE	2865	Evergreen Forest	South
MIDDLE CREEK	3429	Evergreen Forest	South
IDARADO	2987	Mixed Forest	South
LIZARD HEAD PASS	3109	Deciduous Forest	South
SLUMGULLION	3487	Developed, Open Space	South
VALLECITO	3316	Grassland/Herbaceous	South
BEARTOWN	3536	Evergreen Forest	South
RED MOUNTAIN PASS	3399	Deciduous Forest	South
STUMP LAKES	3414	Evergreen Forest	South
CASCADE #2	2719	Mixed Forest	South
COLUMBINE PASS	2865	Deciduous Forest	South
EL DIENTE PEAK	3109	Grassland/Herbaceous	South
LONE CONE	2926	Evergreen Forest	South
SCOTCH CREEK	2774	Evergreen Forest	South
LAPRELE CREEK	2553	Evergreen Forest	North
WINDY PEAK	2408	Evergreen Forest	North
CASPER MTN.	2408	Evergreen Forest	North

WHISKEY PARK	2728	Deciduous Forest	North
SAND LAKE	3063	Evergreen Forest	North
SANDSTONE RS	2484	Deciduous Forest	North
BATTLE MOUNTAIN	2268	Deciduous Forest	North
DIVIDE PEAK	2707	Evergreen Forest	North
RED RIVER PASS #2	3002	Grassland/Herbaceous	South
NORTH COSTILLA	3231	Mixed Forest	South
GALLEGOS PEAK	2987	Mixed Forest	South
CHAMITA	2560	Grassland/Herbaceous	South
BATEMAN	2835	Deciduous Forest	South
HOPEWELL	3048	Grassland/Herbaceous	South
QUEMAZON	2896	Evergreen Forest	South
SENORITA DIVIDE #2	2621	Evergreen Forest	South